Methane Pyrolysis Evaluation for Low-Carbon Hydrogen Production: A Comparative Techno-Economic Analysis

by

Cinthia Victoria Serrato Arias

B.Eng., Universidad Autonoma de Nuevo Leon, 2019

A Research Project Submitted in Partial Fulfillment
of the Requirements for the Degree of

MASTER OF ENGINEERING

In the Department of Mechanical Engineering

Supervisory Committee

Methane Pyrolysis Evaluation for Low-Carbon Hydrogen Production:

A Comparative Techno-Economic Analysis

by

Cinthia Victoria Serrato Arias

B.Eng., Universidad Autonoma de Nuevo Leon, 2019

Supervisory Committee

Dr. Andrew Rowe, Department of Mechanical Engineering, UVic
Supervisor

Dr. Mohsen Akbari, Department of Mechanical Engineering, UVic
Departmental Member

ABSTRACT

In recent years, various hydrogen production pathways have been explored to support net-zero strategies and climate objectives. Methane pyrolysis has emerged as a low-carbon hydrogen technology with promising potential to compete with electrolysis and steam methane reforming processes. This process utilizes thermal decomposition to convert methane into hydrogen gas and solid carbon, effectively avoiding CO_2 emissions during production. A tubular plug flow reactor model was used to evaluate the reactor simulation, focusing on its kinetic parameters and operating conditions. This research evaluates three scenarios, each designed for a hydrogen production capacity of 50 tons per day, exploring two carbon mitigation strategies which are carbon capture and storage (CCS) and the use of an electric arc furnace (EAF). Among these scenarios, Case 1 exhibits the highest environmental impact at 4.14 kg CO_2/kg H_2 due to its lack of decarbonization strategy. A techno-economic assessment reveals that Case 1 has the lowest levelized cost of hydrogen (LCOH) at 2.50 USD/kg H_2, whereas Case 2 with CCS unit presents a LCOH of 2.87 USD/kg H_2, these two options offer competitive hydrogen prices comparable with SMR with CCS. The implementation of EAF in Case 3 exhibits the highest cost at 3.27 USD/kg H_2, although remains more cost-effective than electrolysis. Methane pyrolysis pathway has demonstrated its potential as a viable low-carbon hydrogen production, where Case 2 and Case 3 provide economic feasible option with minimal carbon emissions.

TABLE OF CONTENTS

LIST OF FIGURES

LIST OF TABLES

NOMENCLATURE

C	Carbon
C_A	Concentration of methane gas, mol/m^3
CH_4	Methane
CO_2	Carbon dioxide
D	Reactor internal diameter, m
E_A	Activation energy, kJ/mol
ε	Expansion factor, unitless
F_A	Molar flow rate of methane gas, mol/s
F_{A0}	Initial molar flow rate of methane gas, mol/s
F_B	Molar flow rate of hydrogen gas, mol/s
F_C	Molar flow rate of solid carbon, mol/s
H_2	Hydrogen gas
ΔH_{rxn}	Enthalpy of reaction, kJ/mol
k	Kinetic constant, s^{-1}
k_0	Collision factor, s^{-1}
L	Reactor length, m
P	Pressure, bar
P_0	Initial Pressure, bar
Q	Heat flow, kJ/s
R	Universal gas constant, 8314 J/kmol-K
r_A	Reaction rate law, $mol/m^3/s$
T	Temperature, C
T_0	Initial temperature, C
V	Reactor volume, m^3
v	Volumetric flow rate, m^3/s
v_0	Initial volumetric flow rate, m^3/s
y_{A0}	Initial molar fraction of methane
y_A	Molar fraction of methane
X	Methane conversion

ACRONYMS

BC	British Columbia
CAPEX	Capital expenditure
CCS	Carbon capture and sequestration
CEPCI	Chemical engineering plant cost index
CICE	Centre for innovation and clean energy
D&E	Design and engineering
EAF	Electric arc furnace
FIC	Fixed capital investment
GHG	Greenhouse gas
HHV	Higher heating value, kJ/kg
HTES	High-temperature thermal energy storage
ISBL	Insite battery limit
LHV	Lower heating value, kJ/kg
LMBR	Liquid metal bubble reactor
MEA	Monoethanolamine
NG	Natural gas
O&M	Operation and maintenance
OSBL	Offsite battery limit
PFR	Plug flow reactor
SMR	Steam methane reformation
TDM	Thermal Decomposition of Methane
X	Contingency

ACKNOWLEDGEMENT

I would like to express my deepest gratitude to those who have supported and guided me throughout my master's degree journey. This work would not have been possible without their encouragement, expertise, and unwavering support.

First, I extend my heartfelt appreciation to my supervisor, Dr. Andrew Rowe. Your insightful guidance, patience, and profound knowledge have been instrumental in shaping my research and academic growth. Thank you for believing in me and for providing me with the opportunity to pursue this project.

I would like to thank:

Mr. Luis Herrera, for his patience and support through this project, which encouraged me to continue through my journey.

Mr. Chiradeep Majumder, for his helpful suggestions and support, which greatly encouraged me throughout my studies.

Finally, I would like to thank my family and friends for their unconditional support and understanding throughout this journey. Your love and encouragement have been my constant source of strength.

DEDICATION

This work is dedicated to my parents, Margarita and Victor, who have always trusted me, loved me unconditionally, and encouraged me to pursue happiness and achieve great things. Your unwavering belief in me has been my greatest source of strength.

To my sisters, who showed me new horizons on my journey and inspired me to embrace new challenges with courage and curiosity. To the rest of my family, whose support and love have been a constant comfort and foundation. To my friends, who have stood by me with encouragement, support, and a shared hope for a bright future.

And last, but certainly not least, to my partner, Luis, who has been there for me in every possible way. Our journey has been exhilarating and full of cherished memories and stories. Thank you for being my companion and my greatest source of joy.

Thank you to everyone who has been a part of this incredible journey.

CHAPTER 1: INTRODUCTION

In recent years, hydrogen production technologies are increasingly recognized as critical components in the global energy transition due to their potential to serve as a low-emission energy carrier [1], [2]. Countries such as Canada and the U.S. are seeking viable options to decarbonize their energy systems, and part of this effort depends on reducing their reliance on fossil fuels [3], [4]. Several low-carbon energy carriers have been evaluated in the past few years, including biofuels, synthetic fuels and electricity. Electrification strategies have provided a development on energy transition technologies, such as electric vehicles, yet emissions remain tied to regional electricity sources, posing substantial challenges in fossil fuel-dependent areas [5], [6]. Biofuels, on the other hand, provide a renewable alternative compatible with existing infrastructure, however this approach continues to emit CO_2 during combustion and raise concerns regarding land use, water demand, and food protection [7], [8].

The limitation of electricity and biofuels have brought the opportunity to study other alternatives for low-carbon emission energy fuels such as hydrogen, which has emerged as a prominent clean energy carrier due to its versatility and ability to produce zero emissions at the point of use. Hydrogen can generate electricity in fuel cells with only water as a byproduct, beside this hydrogen can replace natural gas in heat production applications [2]. These two approaches provide versatile solutions for decarbonizing challenging sectors like heavy industry and long-distance transportation [9], [10]. Moreover, hydrogen can be produced from various resources, including natural gas, biomass, and water, making it adaptable to different regions and energy systems. This flexibility is crucial for low emission energy systems, as it offers an alternative to conventional fuels while contributing to energy diversification and security [2].

Although there are several ways to create hydrogen, the two widespread methods are electrolysis and stream-methane reforming (SMR) [11], [12]. Both technologies vary significantly in their chemical conversion, efficiency, and environmental impact [13], [14]. SMR is a well-established process that generates hydrogen by reacting methane with steam at high temperatures, these reactions generate carbon dioxide and carbon monoxide as byproducts. This method is highly efficient in terms of hydrogen yield, but is a major source of CO_2 emissions, making it environmentally costly without carbon capture technologies [12], [15]. Electrolysis, by contrast, involves splitting water into hydrogen and oxygen using electricity, offering a clean alternative when powered by renewable energy. This technology generates zero direct emissions, however its overall efficiency is lower than SMR, particularly due to its significant electricity input [16]. While SMR benefits from lower energy costs, especially in regions with abundant natural gas, electrolysis depends heavily on the cost and availability of renewable electricity [13], [17]. At this moment, SMR remains more economically viable option in the short term, but as renewable energy

becomes cheaper and more widely available, electrolysis is expected to decrease its operating cost in the future [17].

In response to these constraints, recent studies have explored the possibility of producing hydrogen through methane pyrolysis [18], [19], [20]. This process consists of the decomposition of a methane molecule into hydrogen gas and solid carbon, eliminating the release of carbon dioxide at the point of reaction. The solid carbon produced can be stored, utilized in industrial applications, or disposed of with minimal environmental impact [21], [22]. Moreover, methane pyrolysis requires significantly less energy input compared to electrolysis, approaching values that are slightly lower than those of SMR. Consequently, methane decomposition provides a viable and effective alternative for decarbonization [23], [24], offering a more favorable environmental profile than SMR and improved energy efficiency compared to electrolysis.

The methane pyrolysis pathway exists in two main categories: thermal and catalytic. The primary difference between these two options lies in the temperature range utilized for each process. Since thermal pyrolysis relies solely on heat input to break down the methane molecule, it necessitates high operating temperatures, typically above 1000 °C, to achieve a feasible reaction rate [25]. In contrast, the catalytic pyrolysis process is typically conducted at lower temperatures, approximately 800 °C, owing to the incorporation of a catalyst; this improvement reduces operational costs and energy consumption associated with the process [26]. However, catalytic decomposition of methane faces challenges related to reactor design, catalyst deactivation, and product separation [18], [27]. Various approaches have been explored, including solid catalysts, molten metals/salts, and plasma-assisted methods, each with their own limitations [23], [28]. Despite its high energy demands due to the elevated temperatures required, thermal pyrolysis presents advantages in terms of operational simplicity, as it does not rely on additional systems designated to regenerate catalyst.

British Columbia offers a promising environment for methane pyrolysis projects, driven by its abundant natural gas resources, extensive gas infrastructure, and access to low-cost, low-emission electricity [18], [29]. The province’s significant natural gas reserves, supported by established extraction and distribution networks, provide a stable supply foundation for hydrogen production [30]. Furthermore, BC's electricity grid is largely powered by renewable sources, enabling hydrogen production with a minimal carbon footprint [30]. This combination of accessible resources, reliable infrastructure, and clean energy supply positions BC as a favorable region for advancing methane pyrolysis process, enhancing the economic feasibility of low-carbon hydrogen production.

This study conducts a detailed evaluation of methane pyrolysis, focusing on process design and conditions while assessing a techno-economic analysis of various thermal pyrolysis scenarios. By analyzing reaction

kinetics, optimal operating conditions, facility capital and operational costs, resource inputs, and emissions, this assessment aims to clarify the role of methane pyrolysis in providing an economically viable, low-carbon hydrogen production method. Special attention is given to reaction kinetics to understand the optimal operating conditions in a tubular flow reactor. Moreover, three thermal pyrolysis proposals are evaluated to assess the costs associated with the heat source for the pyrolysis reactor. Ultimately, the study seeks to estimate the potential of methane decomposition as a sustainable process option in a future hydrogen economy within British Columbia.

CHAPTER 2: LITERATURE REVIEW

In recent decades, research on methane pyrolysis has expanded significantly, with a focus on overcoming technical challenges that hinder process feasibility, scalability, and industrial implementation. These efforts aim to optimize reaction kinetics and operating conditions, refine reactor design, and improve both energy and resource efficiency, thereby advancing methane pyrolysis as a viable pathway for low-carbon hydrogen production on an industrial scale.

The reaction kinetics present a major challenge in achieving process feasibility, due to its thermodynamic constraints, the uncatalyzed methane pyrolysis reaction is viable only at elevated temperatures. Rodat et al. [31] conducted experimental investigations on the thermal decomposition of methane (TDM) with a 10-kW tubular solar reactor. A parametric analysis was undergone in the range 1500 K – 2300 K (1230 °C – 2030 °C) where a global kinetic expression for the irreversible reaction was identified from the reactor model ($k_0 = 6.6x10^{13}$ s^{-1} and $E_A = 370$ kJ/mol). The proposed plug flow and non-catalytic model showed reasonably good agreement with the experimental results. Similar to Rodat et al., Ozalp et al. [32] studied the solar thermal cracking of methane and the thermal distribution of concentrated solar energy within a plug flow reactor. They suggested a 37-chemical gas-phase reactions mechanism to simulate the non-catalyzed methane cracking, and an 8-chemical surface reactions mechanism for the methane cracking with carbon catalyst. The reversible reaction was first studied by Keipi et al. [33], who carried out experimental research at nominal gas temperatures of 1070 K – 1450 K (800 °C – 1180 °C) in a non-catalytic laboratory test reactor. Their kinetic parameters for the forward ($k_0 = 8.6x10^{12}$ s^{-1}, $E_A = 337$ kJ/mol and a methane coefficient of 1.123) and reverse ($k_0 = 1.1x10^{7}$ s^{-1}, $E_A = 243$ kJ/mol and a hydrogen coefficient of 0.296) reaction were gathered and applied to predict the methane conversion at different temperatures. Trommer et al. [34] evaluated the effect of low methane concentrations ($C_{CH4} = 6.41x10^{-4}$ mol/l) in a direct irradiation vortex flow reactor. Their kinetic analysis assuming a first-decay rate law and plug flow reactor resulted in a 90% chemical conversion at 1500 K (1230 °C) with a residence time of 0.3 s.

Scalability assessments have been conducted on thermal and catalytic methane pyrolysis process, these studies have considered a variety of operating conditions and reactor designs, from simple tubular flow reactor to more complex models such as bubble-liquid based reactors. Catalan et al. [35] evaluated an industrial-scale liquid metal bubble reactor (LMBRs) to produce 200 kt/yr (550 ton/d) of hydrogen, with a reactor size of 96.5 m^3 and a 65% of methane conversion. Their LMBR reactor proposal considered the high temperature (above 1100 °C) molten tin as the liquid metal bath and high operative pressures (above 30 to 90 bar). Their results suggested that a gas hold up of approximately 25% in the liquid bath with a minimum superficial gas velocity of 0.4 m/s. Razmi et al. [36] proposed a novel design for a molten salt

bubble pyrolysis reactor based on concentrated solar energy. The LMBR reactor was modeled as a plug flow reactor with variable density, considering operative conditions of 1200 °C and 1 atm. The implementation of a high-temperature thermal energy storage (HTES) unit was proposed to provide continuous heat input to the pyrolysis reactor. The technical assessment proposed by Razmi et al. considered a facility capacity of 9 t/day, with a low carbon intensity of approximately 2 kg CO_2/kg H_2. Shokrollahi et al. [19] the economic potential of TDM process considering two types of reactor configuration: molten metal-based and thermal plasma-based. Their results reveled that for regions with low carbon intensity for electricity and natural gas, the GHG emissions can fall within the range of 0.76 and 2.58 kg CO_2/kg H_2, when considering direct H_2-fired heating configuration.

Over the past decade, techno-economic analysis has highlighted methane pyrolysis as a promising pathway for cost-effective, low-emission hydrogen production across both large and small-scale configurations. Leal-Perez et al. [37] conducted an economic feasibility analysis for a catalytic pyrolysis facility with a capacity of 65 tons of hydrogen per day, proposing several configurations: solid carbon combustion with CCS and an electric arc furnace reactor. The analysis indicated that both designs yield similar levelized costs of hydrogen (LCOH), at 2.95 and 3.16 €/kg H_2, respectively. Similarly, Parkinson et al. [38] conducted an analysis of a thermal pyrolysis facility utilizing an electric arc furnace, designed to produce 200 kt of hydrogen annually. With a natural gas price of 3 USD/MMBTU, the study estimates a LCOH at 1.72 USD/kg. Another economic study was performed by Razmi et al [36]. Their assessment considered a sensitivity analysis for methane prices ranging from 2 to 10 USD/GJ, resulting in a hydrogen cost of 1.2 to 2.9 USD/kg H_2 respectively. In addition to large-scale, on-site hydrogen production, smaller-scale production configurations also present a cost-effective approach. A mobile autothermal plasma pyrolysis unit was proposed by Tabat et al. [39] with a hydrogen production capacity of 25 kg/h, considering a combination of methane pyrolysis unit with a steam char gasification. The LCOH obtained from this conceptual design ranged from 1.3 to 1.47 USD/kg H_2.

Recent investigations highlight the advantages of hydrogen production through methane decomposition, emphasizing its lower energy intensity and significant reductions in greenhouse gas emissions compared to traditional methods. Diab et al. [24] highlighted that hydrogen produced by methane decomposition presents a significantly lower energy intensity, requiring only 10-30 kWh/kg H_2 compared to 50-60 kWh/kg H_2 for green hydrogen from electrolysis. Their life-cycle assessment also revealed that this method can achieve a reduction in greenhouse gas emissions of 88.3-90.8% relative to conventional grey hydrogen. Al-Qahtani et al. [40] examined an aggregated cost of hydrogen production by accounting for environmental externalities, such as health, ecosystem quality, and resource depletion, to the levelized cost of hydrogen. Their analysis showed that methane pyrolysis has an aggregated cost of 5 USD/kg H_2 with a global warming

potential of 4 kg CO_2/kg H_2 when no carbon mitigation strategy is implemented. Other studies have suggested that gray hydrogen pathways have a higher environmental impact of 10.5 kg CO_2/kg H_2 [37]. Additional research into low-carbon hydrogen production pathways, such as blue and green hydrogen, has also been conducted. Milani et al. [41] found that hydrogen produced from steam methane reforming with CCS, have a levelized cost rage of 1.88 to 2.77 USD/kg H_2, depending on production scale, while electrolysis from PEM technology has a high cost of 6.08 to 7.43 USD/kg H_2 due to its high energy input and low-capacity factor.

CHAPTER 3: METHODOLOGY

3.1 INTRODUCTION

The chapter three outlines the systematic approach taken to model, simulate, and evaluate the proposed methane pyrolysis process for hydrogen production. It describes the essential steps required to achieve the research objectives, from process modeling and data collection to techno-economic assessment. The selected methods were chosen to ensure rigorous analysis, aligning with the objectives of understanding the reactor performance, estimating associated costs, and identifying economic viability within three process design alternatives. This section begins with the process modeling, detailing the reactor modeling, system description and process simulation. Subsequently, the techno-economic assessment methods are discussed, including cost estimation and economic analysis, with a focus on calculating the levelized cost of hydrogen. Lastly, the data collection methods and critical input parameters are presented alongside the software selection used for the study.

3.2 PROCESS MODELING

3.2.1 Methane Pyrolysis Reaction Modeling

This study analyzes the production of 50 tons of hydrogen per day through methane pyrolysis, utilizing natural gas mixture from western Canada. Particularly, the natural gas molar composition of this region consists approximately 95% of methane [42]. The proposed analysis focus on the conversion of this gas, assuming the remaining hydrocarbons to stay inert during the pyrolysis reaction. This simplification facilitates the modeling of the pyrolysis process by removing side reactions and allowing deep analysis of the main driver of hydrogen production.

The pyrolysis reaction consists of the decomposition of one molecule of methane (CH_4) into two molecules of hydrogen gas (H_2) and one molecule of solid carbon (C). This chemical process is performed at elevated temperatures in an oxygen-free environment to prevent combustion. The presented study focuses solely on the thermal decomposition of the methane stream, disregarding the use of catalyst; the overall reaction is shown below.

$$CH_{4\,(g)} \rightarrow H_{2\,(g)} + C_{(s)} \tag{3.1}$$

The proposed pyrolysis model employs a plug flow reactor (PFR) design, as described by **Error! Reference source not found.**. This reactor type is characterized by a continuous flow of reactive mixture, allowing for uniform temperature and concentration profiles along the reactor length. Equation 3.2 establishes the general mole balance at steady state for reactant A, this equation accounts for the conservation of mass inside a tubular reactor, where the difference between the incoming flow rate (F_{A0}) and the outlet flow (F_A) is equal to the consumption of specie A across the reactor volume. The design equation of a plug flow reactor is described in Equation 3.3.

$$F_{A0} - F_A + \int r_A dV = 0 \tag{3.2}$$

$$\frac{dF_A}{dV} = r_A \tag{3.3}$$

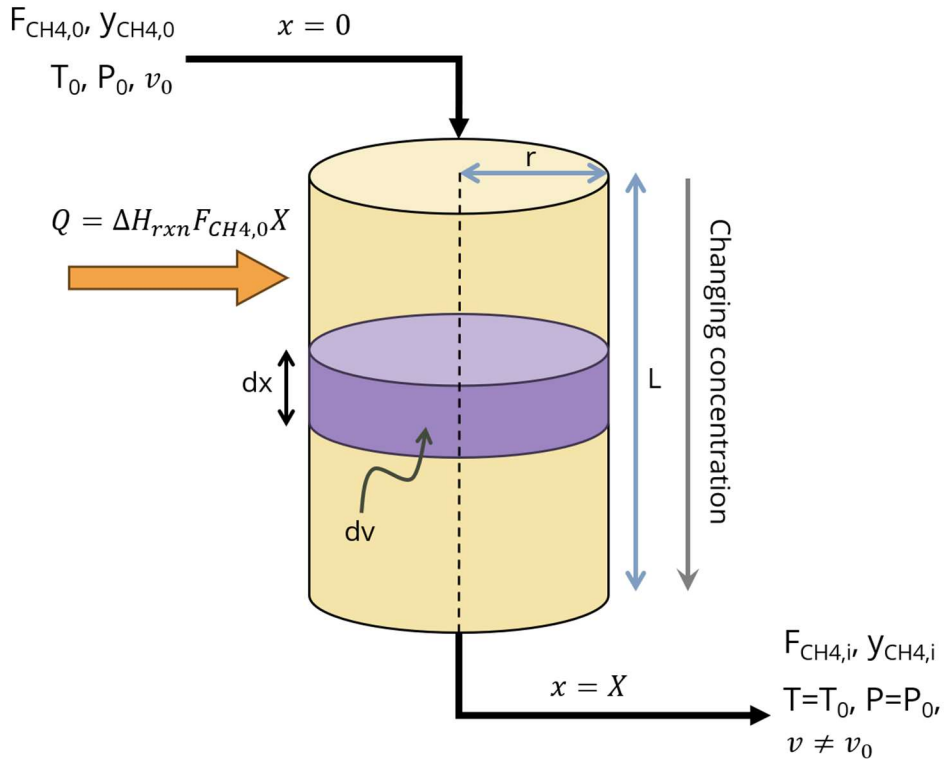

Figure 1. Plug flow reactor schematic model

This evaluation adopts the kinetic model proposed by Rodat et al. in 2009 [31], presented in Equation 3.4. The proposed rate law reflects an irreversible first-order reaction for methane concentration (C_A). Rodat's experimental research identified a collision factor (k_0) of 6.6x10^{13} s^{-1} and an activation energy (E_A) of 370 kJ/mol. To capture the temperature dependence of the kinetic constant (k), Rodat employed the Arrhenius equation, as detailed in Equation 3.5.

$$-r_A = kC_A \tag{3.4}$$

$$k = k_0 \exp\left(\frac{-E_A}{RT}\right) \tag{3.5}$$

The studied methane pyrolysis reaction occurs in gas phase; hence the inclusion of the volumetric flow rate is required to understand the expansion of the gas mixture. Equation 3.6 models the variation of the volumetric flow rate (v) throughout the reaction, considering factors such as methane conversion (X), operating temperature, and pressure. Additionally, this equation accounts for other constant parameters, including the initial volumetric flow rate of the incoming gas mixture (v_0), expansion factor (ε), and initial mole fraction of methane (y_{A0}).

$$v = v_0(1 + \varepsilon y_{A0} X)\left(\frac{T}{T_0}\right)\left(\frac{P_0}{P}\right) \tag{3.6}$$

Equation 3.4 utilizes methane concentration to model the kinetics of the pyrolysis process; however, this approach assumes a constant volumetric flow rate for a gas phase system. Consequently, this assumption can lead to inaccuracies in representing the dynamics of the reaction. To address the previous limitation Equation 3.7 is employed, which address the definition of concentration as the molar flow rate divided by the volume of the gas mixture.

$$C_A = \frac{F_A}{v} \tag{3.7}$$

The molar flow rates of methane, hydrogen, and carbon are determined by the stoichiometry of the reaction and the conversion of methane. Their variation throughout the reaction progression is described by Equations 3.8 to 3.10.

$$F_A = F_{A0}(1 - X) \tag{3.8}$$

$$F_B = F_{A0}(2X) \tag{3.9}$$

$$F_c = F_{A0}(X) \tag{3.10}$$

Equation 3.11 corresponds to the rate law of the methane pyrolysis process under isothermal and isobaric conditions, considering the volumetric expansion of the reaction mixture and the change in moles composition represented by the reactant conversion.

$$-r_A = k\frac{C_{A0}(1 - X)}{(1 + \varepsilon y_{A0} X)} \tag{3.11}$$

This proposed study considers the evaluation of the methane pyrolysis process inside a tubular plug flow reactor in terms of methane conversion, as described in Equation 3.12.

$$F_{A0}\frac{dX}{dV} = -r_A \tag{3.12}$$

The pyrolysis reactor model is derived by combining Equation 3.11 into 3.12, and is presented in Equation 3.13. Equation 3.14 corresponds to the integrated form of Equation 3.13, where V represents the reactor volume required to achieve an specified methane conversion.

$$\frac{dX}{dV} = \frac{-r_A}{F_{A0}} = \frac{k}{F_{A0}}\frac{C_{A0}(1-X)}{(1+\varepsilon y_{A0}X)} \tag{3.13}$$

$$V = \frac{v_0}{k}\left[(1+\varepsilon y_{A0})\ln\left(\frac{1}{1-X}\right) - \varepsilon y_{A0}X\right] \tag{3.14}$$

The thermal decomposition of methane is an endothermic process, necessitating a continuous heat supply to maintain the desired reactor temperature. The required heat input (Q) for the reactor operation is expressed in Equation 3.15.

$$Q = \Delta H_{rxn}\, F_{A0}\, X \tag{3.15}$$

The selection of a plug flow reactor for the methane pyrolysis process has been evaluated by different studies in recent years. This reactor type represents a reliable approach to gas phase reactions due to its continuous flow characteristics, temperature control and smaller equipment size compared to other reactor types. One limitation of PFRs is the potential accumulation of solid carbon on the reactor walls. However, this study assumes that the carbon powder is carried out by the gas flow, disregarding potential deposition inside the reactor.

3.2.2 Process Design and Simulation

This research analyses three process design alternatives for a methane pyrolysis facility capable of producing 50 tons of hydrogen per day. Table 1 list the equipment component required for the three scenarios selected; each option represents a different approach to meeting the heating requirements of the system while aiming to reduce carbon emissions.

Case 1, illustrated in Figure 2, is considered to be base case, in which unconverted hydrocarbon stream, primarily composed of methane, is utilized as a fuel to fulfill the process's thermal energy demand. Case 2

is depicted in Figure 3, this process addresses the opportunities of the base case by incorporating carbon capture and storage (CCS) technology to mitigate carbon emissions generated from using fossil fuels. Finally, Case 3 attends the heating requirements using an electrification approach by replacing the process furnaces with an electric arc furnace reactor (Figure 4), eliminating the reliance on combustion and further reducing the process's emissions. This study reviews each one of the suggested alternatives based on their operational requirements, resource intensity, and economic viability.

Natural gas entering at the battery limit of the facility are assumed to be at 15 °C and 70 bar, these values were gathered from the one of natural gas distributed system in BC region [42]. Major process data and assumptions for the process simulation are listed in Table *2*.

Table 1. Equipment tag list for each case

Equipment Tag	Equipment Description	Case 1	Case 2	Case 3
EA-101	S&T Heat Exchanger	✓	✓	✓
EA-103	S&T Heat Exchanger	✓	✓	✓
EA-104 A/B/C	S&T Heat Exchanger	✓	✓	✓
EA-106	S&T Heat Exchanger		✓	
EA-107	S&T Heat Exchanger		✓	
EA-108 A/B/C	S&T Heat Exchanger		✓	
EA-105	Solex Heat Exchanger	✓	✓	✓
EA-102	Direct-Fired Heater	✓	✓	
PR-101	Pyrolysis Process Furnace	✓	✓	
CYC-101	Solid-Gas Cyclone	✓	✓	✓
K-101 A/B/C	H2 Gas Compressor	✓	✓	✓
B-101	Air Blower 1	✓	✓	
B-102	Air Blower 2	✓	✓	
K-102 A/B/B	CO2 Gas Compressor		✓	
PSA-101	Pressure Swing Adsorption	✓	✓	✓
P-101	Water Pump 1	✓	✓	✓
P-102	Water Pump 2	✓	✓	✓
P-103	Water Pump 3	✓	✓	✓
P-104	Water Pump 4		✓	
SILO-101 A/B/C/D	Hopper Carbon Storage	✓	✓	✓
EAF-101	Electric Arc Furnace			✓
MEA-101	MEA Stripping Column (CCS)		✓	

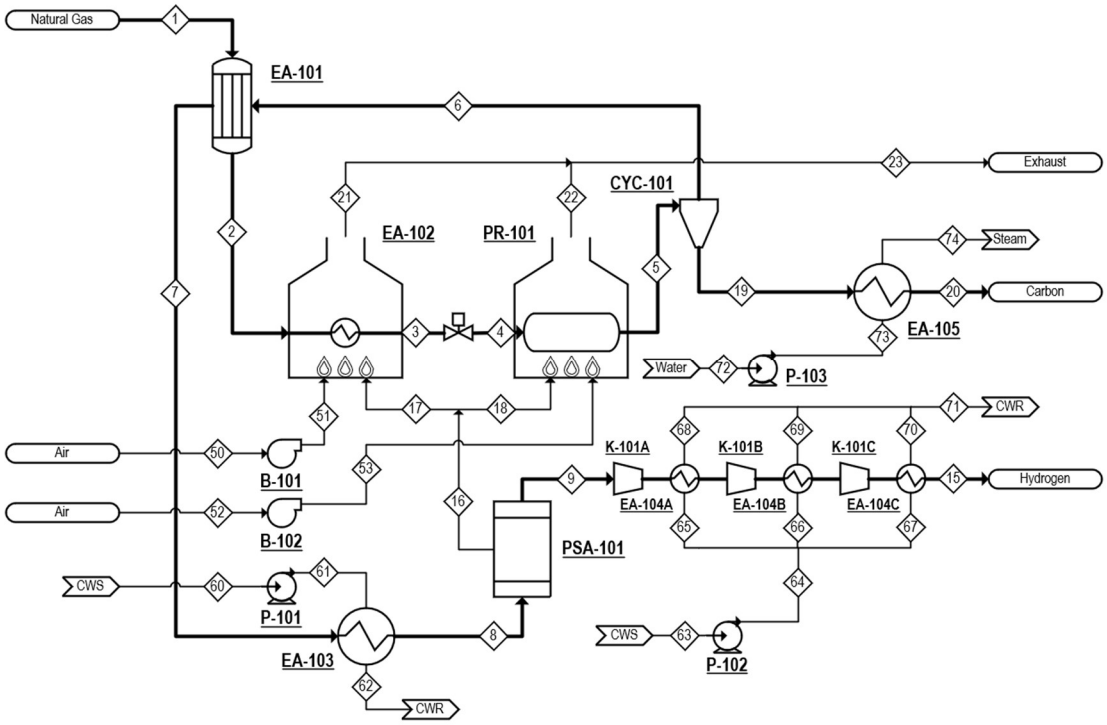

Figure 2. Process flow diagram of methane pyrolysis Case 1

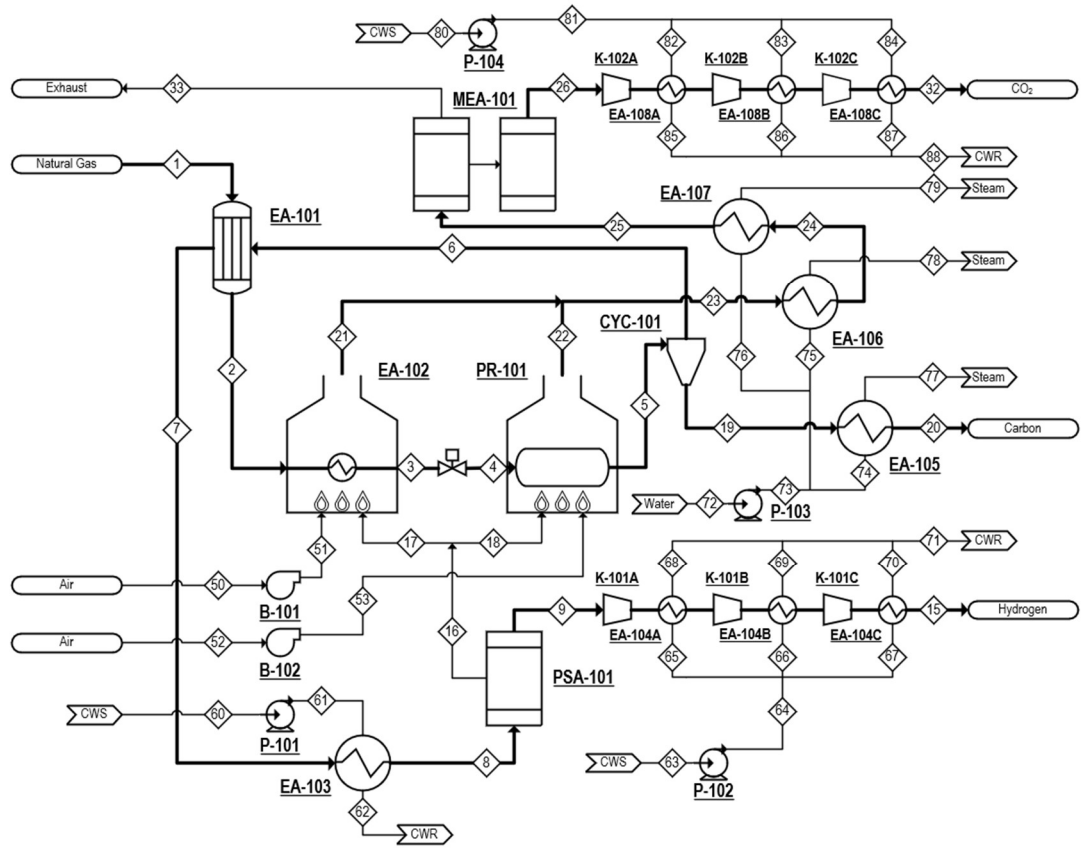

Figure 3. Process flow diagram of methane pyrolysis Case 2

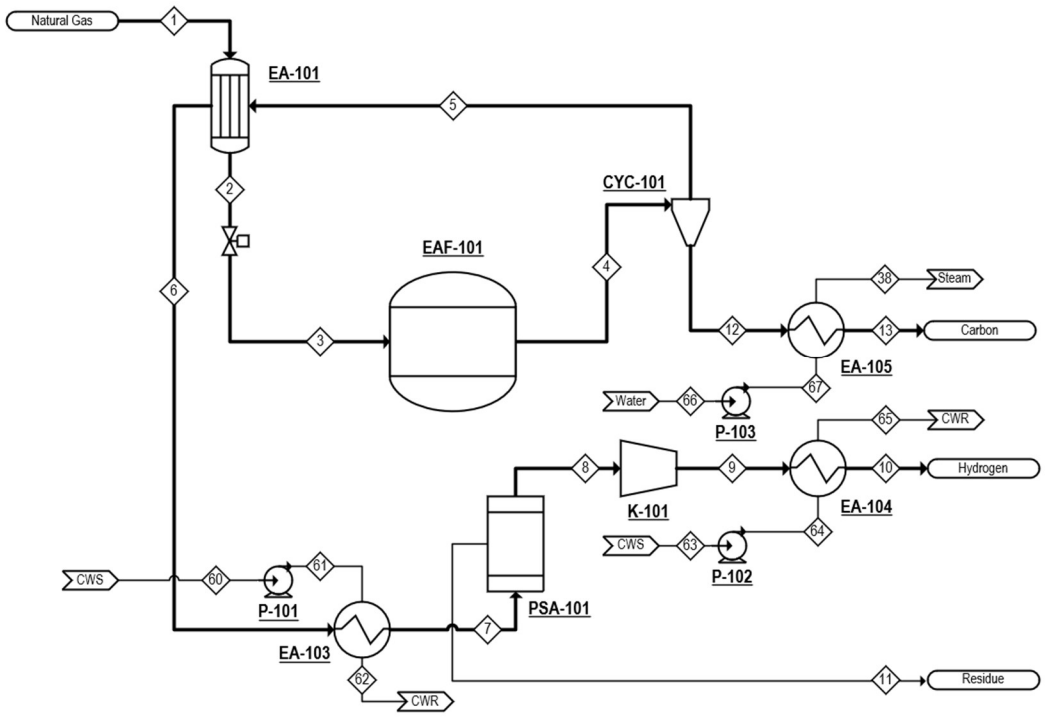

Figure 4. Process flow diagram of methane pyrolysis Case 3

The first step of the methane pyrolysis process is the pre-heating of the natural gas at heat exchanger EA-101. This shell and tube exchanger utilizes the high temperature reactor outlet (stream 6) to pre-heat the feed of natural gas from 15 °C to 800 °C. After EA-101, a second temperature increment is required, in which natural gas enters the process furnace, EA-102, where the temperature rises to 1100 °C. Once the temperature conditioning was completed, the natural gas feed's pressure needed to be adjusted, and a pressure control valve was utilized to decrease its pressure to 10 bar.

Since the pyrolysis reaction is favorable at low pressure, this step was crucial to achieve a high reaction conversion. The operating conditions of the pyrolysis reactor, PR-101, are 1100 °C and 10 bar (stream 4), and the residence time was 2 sec, corresponding to 80% of the methane conversion. No catalyst was used for any of the presented cases in this study, the pyrolysis reactor only evaluates the thermal decomposition of methane molecules, and the remaining hydrocarbons were assumed to be inert during this process. Since the decomposition of methane is an endothermic reaction, a constant heat input is required to maintain the conditions mentioned above, for this reason, the unreacted hydrocarbons present in the gas phase products stream are used to fuel the pyrolysis furnace.

Table 2. Key assumptions implemented in the methane pyrolysis process simulation

Category	Parameter	Values	Units
General	H_2 production rate	50	ton/day
	Atmospheric temperature	15	°C
	Cooing water pump efficiency	75	%
	Cooling water supply temperature	15	°C
	Cooling water return temperature	40	°C
Natural gas pre-conditioning	Natural gas inlet temperature	15	°C
	Natural gas inlet pressure	70	bar
	Pressure control valve outlet	10	bar
	EA-101 tube side outlet temperature	800	°C
	EA-102 process side outlet temperature	1100	°C
	EA-102 furnace efficiency	45	%
	EA-102 furnace excess air percentage	5	%
	Constant operating temperature	1100	°C
Methane Pyrolysis	Constant operating pressure	10	bar
	Methane conversion	80	%
	PR-101 furnace efficiency	45	%
	PR-101 furnace excess air percentage	5	%
	Solid carbon delivery temperature	100	°C
Carbon Conditioning	EA-101 shell side outlet temperature	388	°C
Gas Purification	EA-103 tube side outlet temperature	50	°C
	PSA operating temperature	50	°C
	Percentage of H_2 purity	99.99	%
	H_2 delivery pressure	150	bar
H_2 Conditioning	H_2 delivery temperature	50	°C
	Reciprocating compressor efficiency	75	%
	H_2 compression stages	3	stages
	Pressure ratio for each stage	2.5:1	
	CO_2 storage pressure	110	bar
Carbon Capture Sequestration	CO_2 storage temperature	30	°C
	Reciprocating compressor efficiency	75	%
	CO_2 compression stages	3	stages
	Pressure ratio for each stage	3.8:1	

Upon reaching the reaction step, the reactor's outlet (stream 5) is divided into a gas phase and a solid-carbon phase by CYC-101, process cyclone. The product gas phase outlet (stream 6) consists of mainly hydrogen and a fraction of the unreacted hydrocarbons (methane, ethane, and butane) and other trace compounds. This stream is then used by heat exchanger EA-101, to pre-heat the natural gas feed, while the product stream decreases its temperature from 1100 °C to 388 °C (stream 7). Extra temperature drop is required to maximize the purification stage; therefore, the product gas temperature is further decreased at the EA-103 shell and tube heat exchanger by 50 °C. After the temperature was lowered the purification process is carried out by the pressure swing adsorption, PSA-101. In stream 9, hydrogen outlet is purified by 99.99% and the hydrocarbon traces are collected in the stream 16, this line is then further used as fuel for the process furnace (EA-102) and the pyrolysis reactor (PR-101). Once the purity of the hydrogen stream is achieved, a hydrogen compression step is required to attain its delivery conditions. The pressure conditioning is reached by using a three-stage reciprocating compressor (K-101A/B/C) with intercooling heat exchangers (EX-104A/B/C). Finally, the delivery conditions of hydrogen (stream 15) are 150 bar and 30 °C.

On the other hand, the solid carbon product of the methane pyrolysis reaction (stream 19) is cooled down to 100 °C by a solex heat exchanger (EA-105). Upon reaching the solid carbon delivery temperature (stream 20), the solid particles are stored in four silos for a residence time of 30 days inside the facility.

Three cooling water loops are integrated into the main methane pyrolysis process to provide most of the required cooling. Cooling water supply temperature is assumed to be at 15 °C, these loops are used to decrease the temperature of the process streams at heat exchangers EA-103, EA-104A/B/C and EA-105. The temperature of the cooing water return is considered to be 40 °C, before entering the cooling tower.

The proposal for Case 2 relies on the main steps of Case 1 with the incorporation of a carbon capture sequestration (CCS) unit. The objective of CCS step is to remove the existing CO_2 from the exhaust outlet (stream 23) of PR-101 and EA-102. The temperature of the flue gas stream is approximately 1120 °C; and heat exchangers EA-106 and EA-107 are used to quench its temperature to 500 °C and 50 °C respectively. Subsequently, the flue gases stream needs to be further treated at the CCS unit (MEA-101). Case 2 design incorporates the selection of a monoethanolamine (MEA) as the CO_2 solvent for the chemical absorption column. Then, the MEA-CO_2 mixture enters the regenerator column for MEA solvent recovery, and the CO_2 is purified by the steam condensation at 50 °C. The CO_2 steam is sent to the compression stage to reach its storage conditions. The pressure conditioning is reached by using a three-stage reciprocating compressor (K-102A/B/C) with intercooling heat exchangers (EX-108A/B/C), delivering the CO_2 stream at 110 bar and 50 °C.

In Case 3, the heating requirements for the methane pyrolysis process are met by integrating an electric arc furnace, replacing both the pyrolysis furnace reactor and the direct-fired heater units. This shift avoids the direct combustion of fossil fuels, significantly reducing on-site CO_2 emissions associated with the process. Although CO_2 emissions are not generated directly, the electricity supply of the region is sourced from a mix of renewable and non-renewable sources contributing to its overall emissions. The elimination of combustion systems reduces the need for cooling water to manage high-temperature process streams, minimizing both water usage and cooling system requirements.

3.3 TECHNO-ECONOMIC ASSESSMENT

3.3.1 Fixed Capital Investment Cost

The capital cost estimates for the equipment required in the methane pyrolysis process were determined using cost correlation equations and graphs obtained from multiple sources [37], [43], [44], [45]. Table 3 to 5 provide a summary of the parameters associated with the capital cost estimation for each equipment type. Given that the cost correlations were derived from sources corresponding at different costing years, it was necessary to adjust these estimates to reflect current economic conditions. To achieve this, a cost index adjustment was applied, utilizing the Chemical Engineering Plant Cost Index (CEPCI). This study uses a CEPCI value of 797.9, corresponding to September 2023.

Equations 3.16 to 3.18 present three distinct approaches for estimating purchased equipment costs in USD, referencing the methodologies developed by Sinnott and Towler, Leal-Pérez, and Guthrie, respectively. Finally, Equation 3.19 outlines the formula used to update the purchased equipment costs based on the index ratio, ensuring the accuracy of cost adjustments from historical estimates to current market conditions.

$$C_e = (a + bS^n)\text{*Index} \tag{3.16}$$

$$C_e = C_0\left(\frac{S}{S_0}\right)^f \text{*Index} \tag{3.17}$$

$$C_e = (d \times e)\text{*Index} \tag{3.18}$$

$$\text{Index} = \frac{\text{CEPCI}_{2023}}{\text{CEPCI}_{\text{YEAR}}} \tag{3.19}$$

Table 3. Equipment purchased cost parameter applied on Sinnott and Towler correlation

Equipment type	Parameter, S	Units	a	b	n	Year	CEPCI
Heat Exchanger (U-tube S&T)	Surface area	m^2	24,000	46	1.20	2007	509.7
Pyrolysis Process Furnace	Duty	MW	37,000	95,000	0.80	2007	509.7
Reciprocating Compressor	Driver power	kW	220,000	2,300	0.75	2007	509.7
Air Blower	Air flowrate	m^3/h	3,800	49	0.80	2007	509.7
Water Pumps	Flowrate	L/s	6,900	206	0.9	2007	509.7

Table 4. Equipment purchased cost parameters applied on Leal-Perez correlation

Equipment type	Parameter, S	Units	S0	C0	f	Year	CEPCI
Pressure Swing Adsorption	Purge gas flow	kmol/s	0.294	7.1	0.74	2002	395.6
Solex Heat Exchanger	Solids capacity	ton/h	1,195	10.3	0.60	2016	541.7
Electric Arc Furnace	Net electric power	MWe	175	50	0.60	2016	541.7
MEA CCS Technology	CO_2 captured flow	kg/s	38.4	32.9	0.80	2011	585.7

Table 5. Equipment purchased cost parameters applied on Guthrie correlation

Equipment type	Parameter, S	Units	d	e	n	Year	CEPCI
Solid-gas Cyclone	Solids capacity	ft^3/min	3	8,000	0.80	1969	121
Hopper Carbon Storage	Solids capacity	ft^3	0.9	1,300	0.90	1969	121

To estimate the total cost of the inside battery limit (ISBL) equipment, it was necessary to account for the installation cost in addition to the purchased equipment cost, as described by Equation 3.20. The installation cost is approximated as a factor of the purchased equipment cost and includes estimates for equipment erection, piping, instrumentation, electrical systems, foundations, and labor. For this study, an installation factor of 3.2 was used, which is considered typical for processes involving fluid-solid systems.

The fixed capital investment (FCI) was estimated using Equation 3.21, which incorporates three additional factors: offsite battery limit equipment (OS) costs, design and engineering (D&E) services, and contingency (X). The factors applied for these costs were 0.4, 0.25, and 0.5, respectively. The relatively high contingency factor reflects the inherent uncertainties in the process design, as thermal methane pyrolysis is a novel technology. This consideration help account for potential risks and unforeseen challenges in the implementation of the process at larger scales.

$$C_{\mathrm{ISBL}} = \sum C_e \times 3.2 \tag{3.20}$$

$$C_{\mathrm{FCI}} = C_{\mathrm{ISBL}}(1 + \mathrm{OS})(1 + \mathrm{D\&E} + \mathrm{X}) \quad (3.21)$$

3.3.2 Fixed Operation and Maintenance Cost

Other fixed expenses associated with methane pyrolysis process and any other chemical facility are the fixed operation and maintenance (O&M) costs. These expenses do not vary with the level of production or operation in a facility and are incurred regularly, regardless of the output. The components of fixed O&M costs are detailed in Equation 3.30, and the expenses units are in USD per year. The operating labor cost, presented in Equation 3.22, was extracted from the CICE report, which estimates that operating labor constitutes 1% of the ISBL cost. Equations 3.23 to 3.29, sourced from Sinnott and Towler, outline additional fixed expenses, including operating supervision, direct salary overhead, maintenance, property taxes, insurance, land rent, general plant overhead, and environmental charges.

$$C_{\mathrm{OLAB}} = 1\%\ C_{\mathrm{FCI}} \quad (3.22)$$

$$C_{\mathrm{OSUP}} = 25\%\ C_{\mathrm{OLAB}} \quad (3.23)$$

$$C_{\mathrm{DSAL}} = 40\%\ (C_{\mathrm{OLAB}} + C_{\mathrm{OSUP}}) \quad (3.24)$$

$$C_{\mathrm{MTO}} = 5\%\ C_{\mathrm{ISBL}} \quad (3.25)$$

$$C_{\mathrm{PTAX}} = 1\%\ C_{\mathrm{ISBL}} \quad (3.26)$$

$$C_{\mathrm{LAND}} = 1\%\ (C_{\mathrm{ISBL}} + C_{\mathrm{OSBL}}) \quad (3.27)$$

$$C_{\mathrm{GSAL}} = 65\%\ (C_{\mathrm{OLAB}} + C_{\mathrm{OSUP}} + C_{\mathrm{DSAL}} + C_{\mathrm{MTO}}) \quad (3.28)$$

$$C_{\mathrm{ENV}} = 1\%\ (C_{\mathrm{ISBL}} + C_{\mathrm{OSBL}}) \quad (3.29)$$

$$C_{\mathrm{FO\&M}} = C_{\mathrm{OLAB}} + C_{\mathrm{OSUP}} + C_{\mathrm{DSAL}} + C_{\mathrm{MTO}} + C_{\mathrm{PTAX}} + C_{\mathrm{LAND}} + C_{\mathrm{GSAL}} + C_{\mathrm{ENV}} \quad (3.30)$$

3.3.3 Variable Operation and Maintenance Cost

The variable costs in this analysis are divided into two main categories: the cost of raw materials, primarily natural gas, and the expenses associated with utilities and emissions-related taxes, both of these expenses are expressed in USD per year. The specific market prices used in this study are detailed in Table 7. A

capacity factor (cf) of 0.9 was selected, indicating that the facility is expected to operate for 328 days per year, with the remaining time allocated for scheduled maintenance.

$$C_{\mathrm{VRAW}} = P_{\mathrm{NG}} \times \dot{m}_{\mathrm{NG}} \times cf \tag{3.31}$$

$$C_{\mathrm{H2O}} = cf \times P_{\mathrm{H2O}} \times \sum(\dot{m}_{\mathrm{STEAM}}) \tag{3.32}$$

$$C_{\mathrm{ELE}} = cf \times P_{\mathrm{ELE}} \times \sum\left(\dot{E}_{\mathrm{ELE}}\right) \tag{3.33}$$

$$C_{\mathrm{CO2}} = cf \times P_{\mathrm{CO2}} \times \sum\left(\dot{m}_{\mathrm{CO2,\,FUEL}} + \dot{m}_{\mathrm{CO2,\,ELE}}\right) \tag{3.34}$$

$$C_{\mathrm{WASTE}} = cf \times P_{\mathrm{WASTE}} \times \dot{m}_{\mathrm{C,disp}} \tag{3.35}$$

$$C_{\mathrm{VO\&M}} = C_{\mathrm{CW}} + C_{\mathrm{ELE}} + C_{\mathrm{CO2}} + C_{\mathrm{WASTE}} \tag{3.36}$$

3.3.4 Levelized Cost of Hydrogen

To evaluate the economic viability of the three hydrogen production cases analyzed in this study, a comprehensive framework was established, with the levelized cost of hydrogen (LCOH) chosen as the primary assessment methodology. The LCOH takes into account several critical factors, including capital investment, operation and maintenance expenses, fuel and energy inputs, carbon pricing mechanisms, and the anticipated lifespan of the facility.

$$CRF = \frac{i}{1-(1+i)^n} \tag{3.37}$$

$$\mathrm{LCOH} = \frac{C_{\mathrm{FCI}} \times CRF + C_{\mathrm{FO\&M}} + C_{\mathrm{VRAW}} + C_{\mathrm{VO\&M}}}{\dot{m}_{\mathrm{H2}} \times 8760\frac{\mathrm{hr}}{\mathrm{y}} \times cf} \tag{3.38}$$

Prior to calculating the LCOH for the methane pyrolysis scenarios, the overnight cost of the fixed capital investment must be annualized using the capital recovery factor (CRF), as outlined in Equation 3.37. This factor was determined assuming a facility lifespan, n, of 20 years and a discount rate, i, of 10%. The LCOH, expressed in Equation 3.38, represents the cost per kilogram of hydrogen produced (USD/kg H_2). For this study, the selected facility capacity is 50 tons of hydrogen per day, with a capacity factor of 0.9.

3.4 DATA COLLECTION AND INPUT PARAMETERS

This research assesses the feasibility of integrating methane pyrolysis facilities into the energy infrastructure of western Canada, with a specific focus on British Columbia. To conduct this analysis, key input parameters such as the molar composition, temperature, and pressure conditions of the incoming natural gas stream were obtained from Enbridge Inc.[42], a multinational pipeline and energy company based in Alberta, Canada. Table 6 presents a detailed molar composition of the natural gas mixture used in this research.

Table 6. Natural composition extracted from Enbridge gas

Compound	Formula	mol/mol%
Methane	CH_4	94.6%
Ethane	C_2H_6	4.4%
Propane	C_3H_8	0.2%
n-Butane	C_4H_{10}	0.05%
Nitrogen	N_2	0.4%
Carbon dioxide	CO_2	0.3%
Oxygen	O_2	0.04%
Hydrogen	H_2	0.01%

Table 7. Parameters for the cost estimation

Parameter	Value	Units	Ref.
Natural gas price	3.76	USD / MMBtu	[46]
Cooling water price	1.13	USD / m^3	[46]
Electricity price	4.51	USD / MWh	[46]
Landfill waste tax	50	USD / ton	[43]
Carbon tax	128	USD / tCO_2	[46]
Carbon revenue	188	USD / ton	[46]
Natural gas carbon intensity	60.4	g CO_2 / MJ	[47]
Electricity carbon intensity	9.7	g CO_2 / kWh	[48]
Natura gas LHV	49.05	MJ / kg	[37]

The natural gas and utility prices used in this study were sourced from the BC Center for Innovation and Clean Energy (CICE) 2024 report, which provides region-specific data for British Columbia [49]. Canada

west coast is an ideal location for hydrogen development projects due to its abundant natural gas reserves, clean electricity grid, and water availability. These factors make it a strategic site for methane pyrolysis facilities, as they can help reduce carbon emissions and lower production costs. Table *7* presents the list of assumptions based on the data collected for the region. Additionally, the carbon intensity values for natural gas and electricity are specific to BC, reflecting the province's unique energy profile. A carbon tax of 170 CAD (128 USD) per ton of CO_2 emissions is assumed for this study, this value corresponds with the projected carbon tax for 2030 [50]. While the current federal carbon tax in Canada stands at 65 CAD per ton of CO_2, this higher assumption reflects future policy expectations.

3.5 SOFTWARE SELECTION

This study aims to provide a proposal for a 50 tons/day of hydrogen facility. The methane pyrolysis process consisted of three main stages: preconditioning of the natural gas, the pyrolysis reaction, and the purification and conditioning of the products (hydrogen and carbon).

The process simulation of the thermal decomposition of methane was conducted using Aspen Hysys version 8.8, a process simulation software widely recognized for its process modeling, and sensitivity analysis of critical parameters. The Peng-Robinson property package was chosen as the equation of state due to its robustness in handling the thermodynamic properties of the lightweight hydrocarbon compounds present in the natural gas feed stream.

Previous process simulation studies have demonstrated the application of this software in steam methane reforming [51], [52], biomass gasification [53], [54], and more recently, in developing proposals for methane pyrolysis processes [37], [55].

For the pyrolysis reactor simulation, a one-dimensional plug flow reactor model was utilized to capture the dynamics of the methane decomposition process. Detailed equipment modeling was conducted using MATLAB version R2023a relying on its powerful computational capabilities.

CHAPTER 4: RESULTS

4.1 REACTOR MODELING

This study utilizes the reaction rate law and kinetic parameters reported by Rodat et al. [31], this proposal relies on the thermal cracking of the C-H bonds of the methane molecule. For this reason, elevated reaction temperatures, particularly above 547 °C [49], are necessary to make this process thermodynamically feasible. To determine the optimal operating temperature for methane pyrolysis, a range of temperatures from 900 °C to 1200 °C was analyzed. Although a 100% of methane conversion can be ideally achieved at high temperatures, this study considers an 80% of conversion due to possible reaction inefficiencies regarding mass and heat transport. Figure 5 illustrates the relationship between volume of the reactor and methane conversion at different conditions. At 900 °C, the required reactor volume was found to be excessively large, approximately 2,000 m^3, making the construction impractical. On the contrary, temperatures above 1100 °C resulted in minimal reactor volumes, which would complicate reactor operation due to control and safety challenges.

A more realistic outcome was observed at 1000 °C and 1100 °C, where the reactor volumes were more manageable. However, at 1000 °C, the required volume was still larger than desired for practical operation, approximately 110 m^3. Based on these findings, a temperature of 1100 °C was selected, as it offered a feasible reactor volume of approximately 9.25 m^3. This temperature also aligns with typical operational conditions for thermal decomposition processes in methane pyrolysis presented in the literature [26].

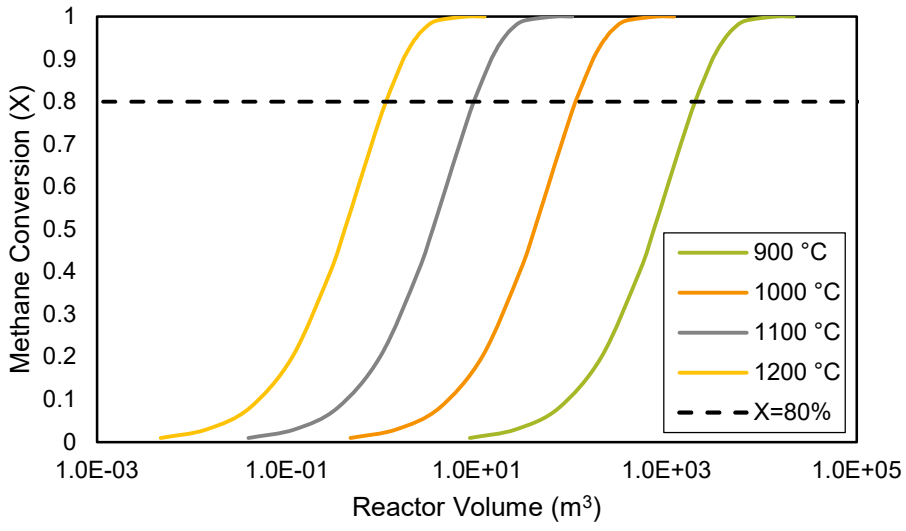

Figure 5. Pyrolysis reactor volume estimated at different temperatures and methane conversions

The temperature dependence of the kinetic constant was also evaluated, these results are presented in Figure 6. As described by Arrhenius equation, higher operating temperatures lead to an exponential increase in the kinetic constant, accelerating the reaction rate. At 1100 °C, the kinetic constant was found to be 0.55 s^{-1}, these values were used for the subsequent evaluation of the kinetic reaction of the methane pyrolysis.

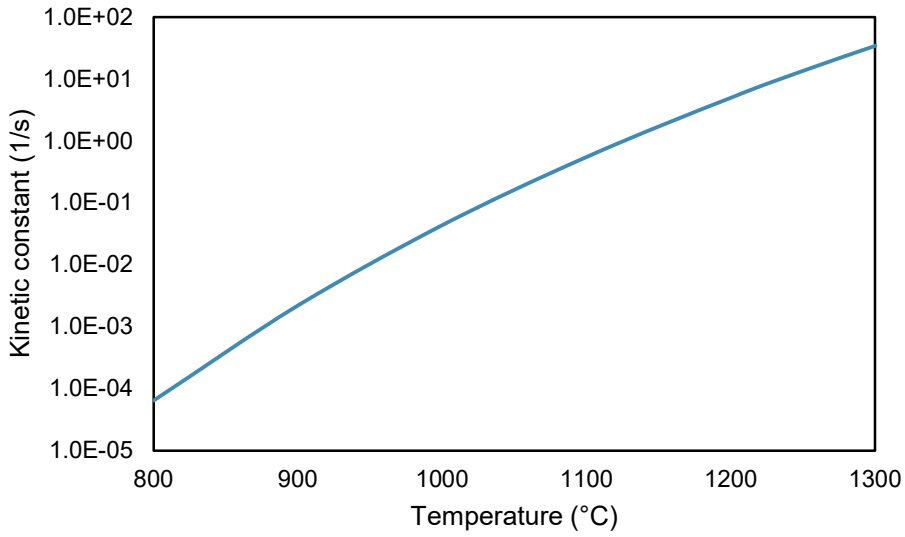

Figure 6. Kinetic constant of pyrolysis reaction at different temperatures

This study evaluates the impact of incorporating the expansion factor on the reaction rate law, as expressed in Equation 3.11. In this evaluation, it is assumed that volumetric flow rate of the reactive mixture changes during the pyrolysis process. Some studies overlook the influence of this effect on the reactor performance. This research found that accounting for this parameter yields valuable insights and supports the development of a more accurate reactor model.

Figure 7 shows the effect of the expansion factor across the reactor volume. When the expansion factor is considered ($\varepsilon = 1$), the density of the gas mixture changes, the reason behind these results establishes that the number of the gas molecules inside the mixture is increasing, as one molecule of methane is consumed when two molecules of hydrogen are produced. Finally, this change in the molar flow rate expands the volumetric flow of the mixture. When the expansion factor is not considered ($\varepsilon = 0$), the volumetric flow rate remains constant as specified in Equation 3.4.

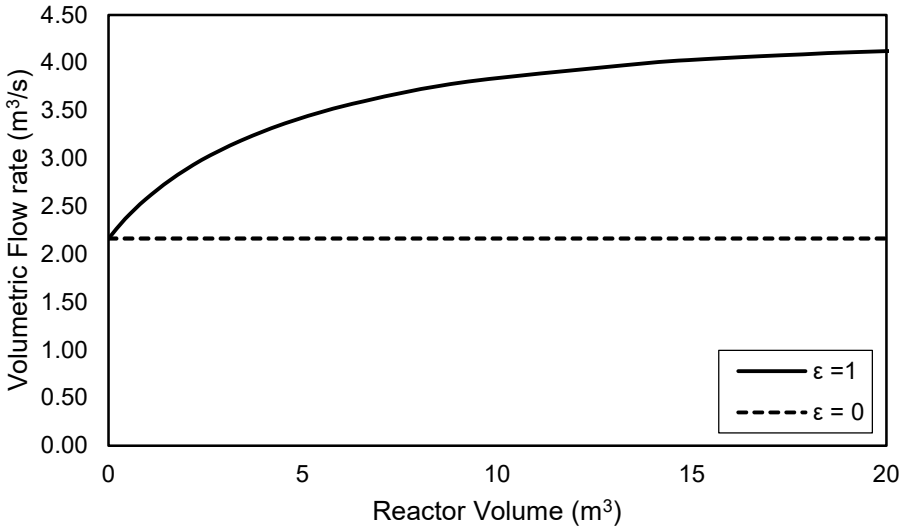

Figure 7. Volumetric flow rate change across the reactor volume.

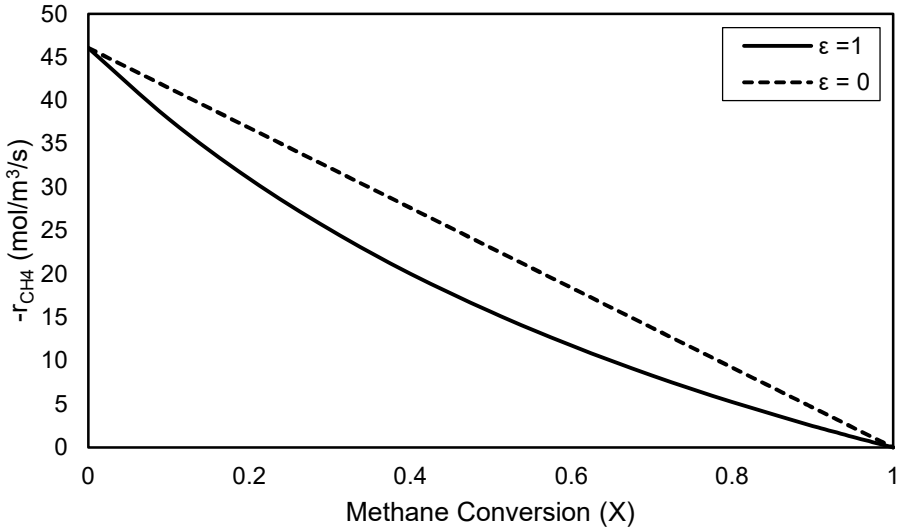

Figure 8. Effect of expansion factor on methane pyrolysis rate law

The introduction of the expansion factor establishes nonlinear behavior in the reaction kinetics, as illustrated in Figure 8. In a first-order reaction with a constant volumetric flow rate, the rate law is directly proportional to the conversion of methane. However, when the expansion factor ($\varepsilon = 1$) is accounted for, an additional conversion term appears in the denominator of the rate law expression at Equation 3.13. This modification shifts the original first order kinetics from a linear to a logarithmic trend. Consequently, the expansion factor presents an effect in slowing the reaction rate by altering the flow dynamics within the reactor.

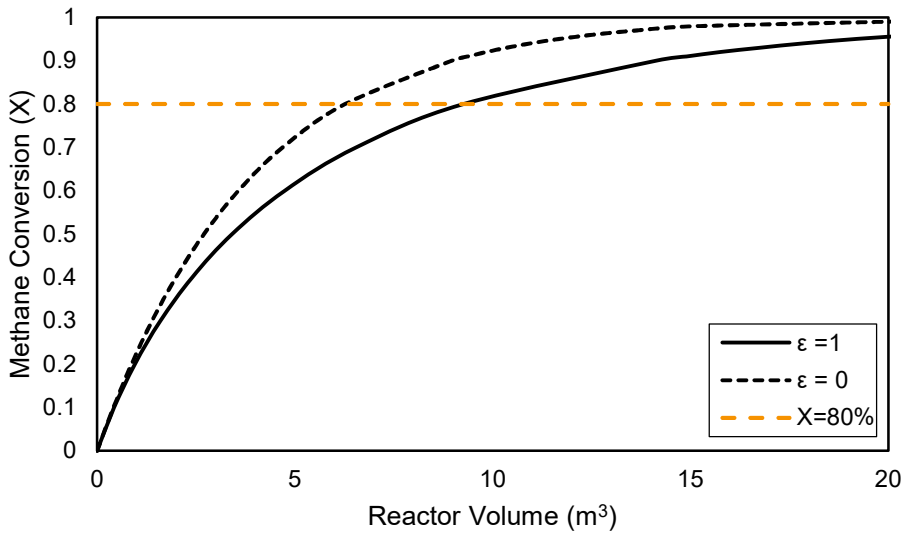

Figure 9. Effect of expansion factor on methane conversion throughout reactor volume

Figure 9 illustrates the methane conversion as a function of reactor volume. As described in Figure 8, changes in volumetric flow rate due to the expansion factor slow the reaction rate. This effect is evident in the reactor volume required to achieve 80% conversion. Once the expansion factor ($\varepsilon = 1$) is considered, the required reactor volume is 9.25 m^3. In contrast, without accounting for this parameter, the required volume decreases to 6.3 m^3.

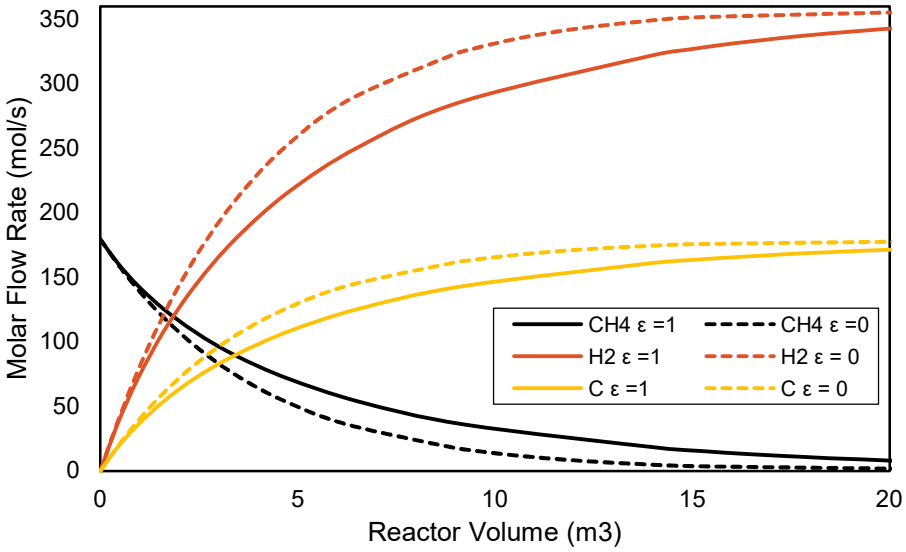

Figure 10. Molar flow rate of reactive species across reactor volume

The impact of the expansion factor is also reflected in molar flow rate of reactive species, as presented in Figure 10. The incoming natural gas flow rate is approximately 190 mol/s, with a methane molar

composition of 94.6%. The remaining 4.4% consists of other light hydrocarbon species that are assumed to remain inert under the given conditions. At approximately 9 m^3 of reactor volume, the production of hydrogen gas is 287 mol/s of hydrogen, equivalent to 50 t/day. Similarly, the formation of solid carbon increases throughout the reactor, reaching a production rate of 144 mol/s at 80% conversion. As shown in Figure 9, achieving the desired molar flow rates for both hydrogen and carbon will require a larger reactor volume to accommodate the expansion caused by the new gas molecules created.

4.2 THERMODYNAMIC PROCESS ASSESSMENT

This study conducts a thermodynamic assessment of the three proposed cases to compare and evaluate their respective advantages, disadvantages, and operational characteristics. To enable a consistent analysis across the various process designs, each facility is assigned the same hydrogen production capacity and methane conversion at the pyrolysis reactor. The principal findings are summarized in Table 8.

Table 8. Thermodynamic performance of the methane pyrolysis scenarios

Process Parameter	Units	Case 1	Case 2	Case 3
NG flow rate	kg/s	3.20	3.20	2.40
NG thermal input	MW	158.58	158.58	119.14
H_2 mass flow rate	t/day	50.0	50.0	50.0
Reactor temperature	°C	1100	1100	1100
Reactor pressure	bar	10	10	10
Power requirements breakdown				
Air blowers	MW	1.15	1.15	0.00
H_2 compressors	MW	3.25	3.25	3.25
CO_2 compressors	MW	0.00	0.78	0.00
Pumps	MW	0.02	0.03	0.02
Electric arc furnace	MW	0.00	0.00	17.75
Other auxiliaries	MW	0.00	0.00	0.30
Net electric power	MW	4.42	5.21	21.32
Water requirements breakdown				
Steam exports	kg/s	0.97	7.81	0.97
Plant index				
H_2 efficiency	$H_{2,\,LHV}/NG_{LHV}$	0.44	0.44	0.58
H_2 yield	mol_{H2}/mol_{CH4}	1.60	1.60	2.08
Resource Input				
Natural gas input	kg_{CH4}/kg_{H2}	5.53	5.53	4.15
Electricity input	kWh_e/kg_{H2}	2.12	2.50	10.23
Water input	kg_{H2O}/kg_{H2}	1.67	13.50	1.67
Facility emissions				
Electricity upstream emissions	kg_{CO2}/kg_{H2}	0.02	0.03	0.12
On-site facility emissions	kg_{CO2}/kg_{H2}	4.11	0.00	0.00
Total facility emissions	kg_{CO2}/kg_{H2}	4.14	0.03	0.12

The results in Table 8 provide insights into the process specifications, electricity demand, water requirements, natural gas consumption, as well as resource efficiency and facility emissions. Cases 1 and 2 exhibit identical natural gas flow rates and thermal inputs, corresponding to 3.2 kg/s and 158.6 MW respectively. These cases also operate at 1100 °C and 10 bar at the pyrolysis reactor, with a methane conversion of 80%. On the other hand, Case 3 demonstrates a distinct process configuration, with a 25% reduction in both natural gas feed stream (2.4 kg/s) and thermal input (119.1 MW), attributed to the recirculation of unreacted hydrocarbons. This recirculation reduces the demand for fresh natural gas while preserving the same hydrogen production capacity and reactor conditions.

Regarding the power requirements, the highest net power electric demand is found in Case 3. This is because of the addition of electric arc furnace technology, which increases power requirements, with the furnace consuming 17.75 MW. This results in a significantly higher net electric power demand of 21.32 MW for Case 3, compared to 4.42 MW for Case 1 and 5.21 MW for Case 2. The other two designs present similar demands across components, with air blowers requiring 1.15 MW, hydrogen compressors 3.25 MW. Case 2 differs from Case 1 on its addition of carbon capture unit, in order to store CO_2 a compression stage needs to occur, adding a 0.78 MW to its electricity demand.

In terms of water input requirements, with Case 2 shows a significantly higher demand at 13.50 kg of water per kg of H_2, contrasting with 1.67 for Cases 1 and 3. This water demand only considers the cooling water flow rate used to produce steam in EA-105, EA-106 and EA-107. Additionally, Case 2 also have the larger cooling water loop system requirement due to cooling the extra heating demand required by its extra heat exchangers. Although, Case 2 might seem to have a relatively high-water requirement when compared to other methane pyrolysis design, this value is considered low against other hydrogen production technologies such as steam methane reforming and electrolysis with a 19 and 16.5 kg H_2O per kg CO_2, respectively [49].

Facility emissions are categorized into upstream emissions from electricity generation and direct emissions produced on-site by each facility. Case 1, which lacks a decarbonization strategy, presents a substantial on-site facility emissions of 4.14 t CO_2 per kg of H_2, making it the least effective option for CO_2 mitigation. By contrast, Case 3 shows higher upstream emissions compared with the other two scenarios, reaching 0.12 kg CO_2 per kg of H_2 due to its elevated power consumption. Both Cases 2 and 3 effectively reduce in-site facility emissions to zero due to decarbonization strategies, leading to significantly lower total facility emissions.

This study considers Case 2 as the most favorable methane pyrolysis design strategy. Despite its relatively higher water requirements for cooling, this case demonstrates notable advantages in emissions reduction

by incorporating a carbon capture system. This design also maintains resource efficiency with a comparable natural gas input to Case 1. Compared to Case 3, which incurs high power demands due to the electric arc furnace, Case 2 achieves a lower overall electric demand, resulting in minimized upstream emissions. These combined attributes position this alternative as the optimal choice for sustainable hydrogen production through methane pyrolysis.

4.3 TECHNO-ECONOMIC ASSESSMENT

The results of the techno-economic assessment for the three scenarios proposed in this study, are presented in Table 9. This analysis considers the fixed and variable cost associated with the facility, to further evaluate the levelized cost of the hydrogen made by each methane pyrolysis design.

Table 9. Cost breakdown of fixed and variable expenses, and LCOH for each case study

Process Stage	Units	Case 1	Case 2	Case 3
NG pre-conditioning	M USD (%)	2.52	2.52	2.19
Pyrolysis reaction	M USD (%)	5.42	5.42	59.45
Gas purification	M USD (%)	10.29	10.29	8.92
H_2 Conditioning	M USD (%)	10.46	10.46	10.46
C Conditioning	M USD (%)	6.11	6.11	6.11
Carbon capture	M USD (%)	0.00	30.87	0.00
Fixed and Variable Cost Breakdown	Units	Case 1	Case 2	Case 3
Fixed capital investment cost	M USD/y	10.02	18.90	25.07
Fixed O&M cost	M USD/y	3.05	5.24	6.75
Variable raw material (NG) cost	M USD/y	15.88	15.88	11.93
Variable O&M cost	M USD/y	12.74	4.60	10.28
- Electricity	M USD/y	1.57	1.85	7.56
- Water/Steam	M USD/y	0.03	0.25	0.03
- Landfill disposal	M USD/y	8.69	0.06	0.24
- Carbon tax	M USD/y	2.45	2.45	2.45
Levelized Cost Of Hydrogen	Units	Case 1	Case 2	Case 3
LCOH, fixed	USD/kg H_2	0.80	1.47	1.94
LCOH, variable	USD/kg H_2	1.74	1.25	1.35
LCOH, total	USD/kg H_2	2.54	2.72	3.29

Table 10. Methane pyrolysis stage and equipment list

Process Stage	Equipment Tag	Process Stage	Equipment Tag
NG pre-conditioning	EA-101	Carbon capture	EA-106
	EA-102		EA-107
	B-101		MEA-101
	K-103		K-102A/B/C
Pyrolysis reaction			EA-108A/B/C
	PR-101	C Conditioning	EA-105
	CYC-101		P-103
	B-102		SILO-101A/B/C/D
Gas purification	EA-103	H_2 Conditioning	K-101A/B/C
	PSA-101		EA-104A/B/C
	P-101		P-102

Table 10 categorizes the inside battery limits (ISBL) equipment into the main process categories: natural gas (NG) pre-conditioning, pyrolysis reaction, gas purification, hydrogen conditioning, carbon conditioning, and carbon capture. The total ISBL equipment cost is shown in Figure 11, where facility equipment costs are allocated across the main process stages. These values account for not only the purchase cost of equipment but also installation expenses. Appendix B presents the costing breakdown for each piece of equipment in the three proposals.

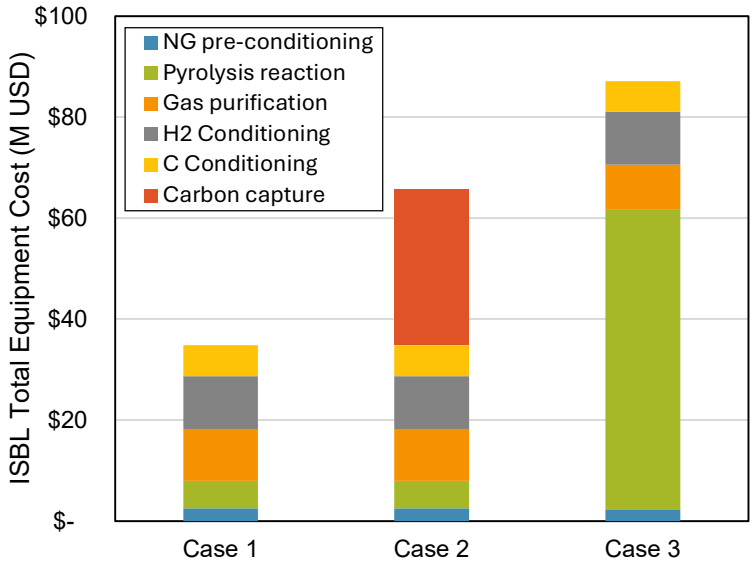

Figure 11. ISBL Total equipment cost per methane pyrolysis scenario

The cost evaluations for Cases 1 and 2 are nearly identical, as Case 2 builds upon Case 1 by incorporating a carbon capture system, which adds an additional cost of 30.87 million USD. The substantial expense of the CCS is primarily due to the monoethanolamine unit (MEA-101) and CO2 compressors (K-102), which together account for 95% of the total cost of this stage. The cost of NG pre-conditioning remains relatively consistent for the three scenarios, with Case 1 and 2 at 2.52 million USD, while Case 3 shows a slight decrease to 2.19 million USD, due to removal of the direct fired heater furnace and its corresponding air blower. The pyrolysis reaction stage, however, displays significant difference between the proposals. In Cases 1 and 2, the reactor considers a pyrolysis furnace with direct-fired heater unit attached, the sum of this stage is expected to cost 5.42 million USD. For Case 3, the methane pyrolysis reaction takes places in an electric arc furnace with a total process stage cost of 59.45 million USD, the cost of this equipment is substantial compared to the rest of the facility units.

Gas purification costs are also significant due to the presence of pressure swing adsorption (PSA) unit, with 10.29 million USD allocated in both Cases 1 and 2, while Case 3 has a reduced cost of 8.92 million USD. This cost difference for Case 3 reflects the recirculation of the unconverted methane to the NG feed stream, which decrease the amount of purge gas at the PSA unit. The hydrogen conditioning step accounts for the compression and cooling of the hydrogen stream, the cost associated with this stage accounts for 10.46 million USD for all cases, as the three proposals provide the same hydrogen capacity. Similarly, carbon conditioning stage costs are uniform, with each case allocating 6.11 million USD.

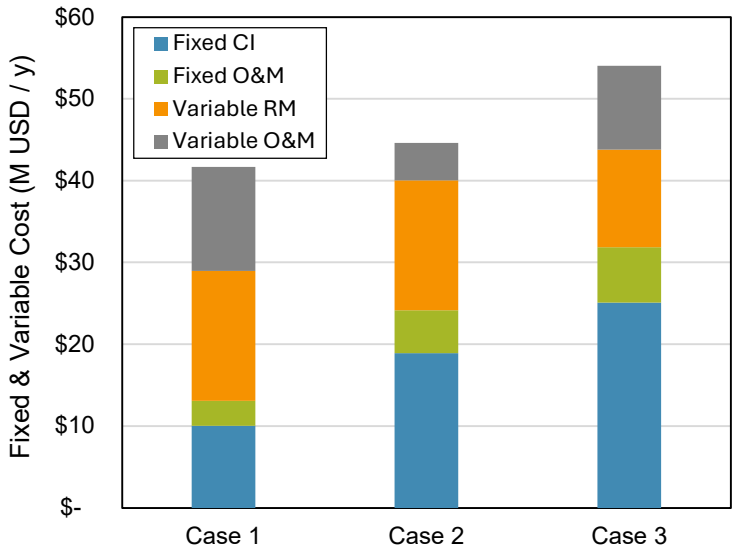

Figure 12. Fixed and variable cost associated with each scenario

The main assumptions made for the market evaluation consisted of a NG price of 0.23 USD/kg, an electricity price of 45 USD/MWh, a utility water price of 1.13 USD/m^3, a carbon tax of 128 USD/kg, and

a landfill disposal of 50 USD/ton. Figure 12 presents the fixed and variable costs for the three cases showing distinct differences on capital investment, operational expenses, and resources usage. Case 1 presents the lowest fixed capital investment cost at 10.02 million USD/y, while Case 3 incurs the highest investment cost at 25.07 million USD/y. The fixed operating and maintenance (O&M) costs are directly related with capital investment; hence Case 1 presented the lowest cost option, followed by Case 2 and lastly Case 3.

In terms of variable costs, the raw material cost accounts solely for natural gas purchase, this value remains the same in Cases 1 and 2 at 15.88 million USD/y, while Case 3 benefits from the NG recycle, with a cost of 11.93 million USD/y. Regarding the variable O&M cost, Case 1 has the highest cost at 12.74 million USD/y, largely due to higher carbon tax expenses. Case 2, with its carbon capture system, sees a significantly lower variable O&M cost of 4.60 million USD/y, as it generates less CO_2 emissions. Case 3 uses a substantial amount of electricity which affects its utilities expenditure, reaching a 10.28 million USD/y.

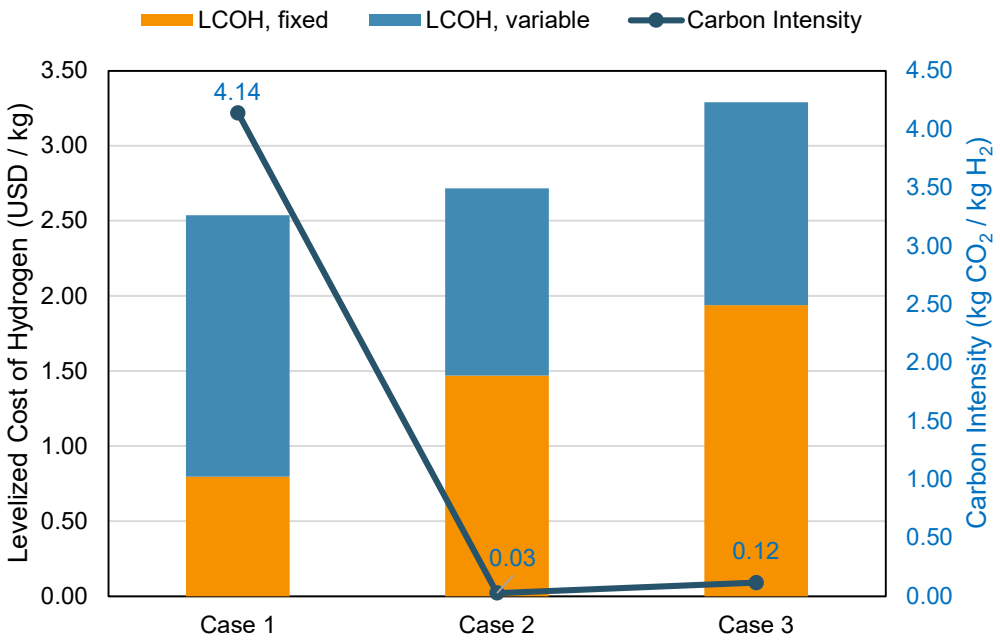

Figure 13. Levelized cost of hydrogen for each methane pyrolysis case

Finally, the levelized cost of hydrogen is analyzed in Figure 13, where the three scenarios are compared to evaluate the most economic low-emission option. Case 1 does not include any decarbonization strategy, however its hydrogen production cost was estimated to establish the minimum LCOH at 2.54 USD/kg H_2, consisting of a fixed cost of 0.80 USD/kg H_2 and a variable cost of 1.74 USD/kg H_2. Case 2 introduces a carbon capture system, resulting in a slightly higher LCOH of 2.72 USD/kg H_2. This increase is attributed primarily to a rise in fixed costs at 1.47 USD/kg H_2, while variable costs decrease to 1.25 USD/kg H_2 due

to CO_2 emission reduction. Case 3, which employs an electrification approach, have a total 3.29 USD/kg H_2, the highest among the proposed options. Similar to Case 2, this price is driven by higher fixed costs of 1.94 USD/kg H_2, while variable costs are somewhat reduced to 1.35 USD/kg H_2. The results provided in Figure 13, underscore the financial trade-offs involved in choosing a decarbonization strategy for hydrogen production, with Case 2 emerging as the most economical low-emission option.

CHAPTER 5: DISCUSSIONS

5.1 LIMITATIONS

The thermal decomposition of methane was studied in a plug flow reactor at elevated temperatures. High reaction rate and methane conversion could be achieved at 1100 °C and 10 bar. However, the rate law model proposed by Rodat et al. disregards the analysis of mass and heat transport inside the reactor. Particularly, solid carbon management reflects a challenge for plug flow reactor designs. According to experiments conducted by previous authors, part of the carbon product expected to adhere to the reactor chamber walls. If the thickness of this layer is not controlled, it could hinder the reactor's heat supply, and eventually leading to clogging the reactor outlet. This constrains in the analysis imposes inefficiencies in the total conversion of the methane. As a result, this study proposed a moderate methane conversion of 80% for the subsequent analysis, however lower conversion values can be expected depending on reactor's design and performance operation.

The current thermodynamic system analysis includes several limitations that could be addressed in future work to provide a more accurate representation of process operations. First, the reactor heat input efficiency is currently simplified, as direct conversion from electrical to thermal energy was assumed for Case 3, on the other hand Case 1 and 2 presented a direct transfer of combustion heat to thermal input. In practice, this conversion is not 100% efficient, and real systems experience heat losses and equipment inefficiencies that should be accounted for to provide a more accurate energy assessment. Second, the pressure swing adsorption unit considered an ideal hydrogen separation from the gas mixture. However, in real applications this process presents some limitations as part of hydrogen gets trapped in the adsorbent and is then further disposed with the rest of the unconverted hydrocarbons. This inefficiency in the separation process might cause a substantial increase on the natural gas input depending on the unit performance.

As the methane pyrolysis reaction represents a novel process that has yet to be scaled, there are inherent uncertainties concerning the cost and design of the primary equipment. This study assumes that Cases 1 and 2 utilize the same reactor design, incorporating a combination of a direct-fired heater unit for the pyrolysis reactor. The cost estimation for this equipment was derived from a standard process furnace heater, adjusted with a proposed correction factor. However, it is suspected that the cost estimation might have underestimate the actual expenses associated with this unit, given that novel technologies are likely to incur in higher capital costs. In contrast, Case 3 calculates the cost of the electric arc furnace based on an external reference; the result of this estimate presents the highest capital investment for an equipment which is likely to be correct. Although it is expected that this unit will become more cost-effective in the future.

5.2 FUTURE WORK

To enhance the accuracy and applicability of this reactor model, future studies could incorporate additional analysis, such as pyrolysis of other hydrocarbon compounds, recycle of unreacted hydrocarbons and catalyst implementation. This research focuses solely on the decomposition of the methane molecule, although natural gas mixtures typically contain a variety of light hydrocarbons like ethane, propane and butane. The pyrolysis of these additional compounds was not considered in this study. Future work on reactor modeling should incorporate a more complex pyrolysis mechanism to further represent the actual process operation and heat demand.

The present study evaluates the unconverted hydrocarbon recycle only in Case 3 proposal. This modification reduces the natural gas input to the process, making it more resource efficient. By contrast, Cases 1 and 2 were not considered for recycle implementation under the current evaluation. Future investigations should explore this alternative with other pyrolysis proposal, especially those with low reaction conversion. This research explores primary the thermal methane pyrolysis process, however incorporating catalytic pyrolysis into the analysis could help reducing energy demand by lowering the operational temperature of the reactor.

To improve the techno-economic assessment of this project, several evaluations are recommended for future research. First, conducting a sensitivity analysis on key variables such as natural gas price, electricity cost, and carbon tax would provide a more comprehensive understanding of these factors and their ability to reflect characteristics of different economic regions and markets. Additionally, it is suggested to incorporate a parameter evaluation for contingency costs and facility lifetime, as these elements significantly influence the financial feasibility of the projects.

A different proposal for future work considers the scaling effects of the hydrogen capacity in a methane pyrolysis facility. A baseline production of 50 tH_2/day was assumed for the study, however, it is expected that at higher facility capacities the levelized cost decreases. Another area for improvement involves incorporating location factor into the fixed capital investment cost, this parameter accounts for the shipping costs associated with facility components, as these adjustments would reflect the geographical influence on the project.

CHAPTER 6: CONCLUSION

Several hydrogen production pathways have been studied over the last decade to support net-zero strategies and climate objectives. Methane pyrolysis is an emerging technology with promising potential in the hydrogen market, positioned between electrolysis and steam methane reforming (SMR). This process relies on the thermal decomposition of the methane into hydrogen gas and solid carbon, thereby avoiding generation of CO_2 during the reaction process. The presented project evaluates the pyrolysis reaction in a tubular plug flow reactor model, analyzing its kinetic parameters and operating conditions. Elevated temperatures, around 1100 °C, are required to promote reaction rate, decrease reactor volume and achieve high hydrogen yields. The reactor model proposed exposes some limitations related with carbon management and heating supply, thereby is suggested that different reactor designs can improve these technical challenges.

To further analyze the thermal methane pyrolysis process, this study compares three different proposals, each with a hydrogen capacity of 50 tons per day. Case 1 serves as the baseline option, representing conventional methane pyrolysis without any decarbonization strategy implemented. In contrast, Case 2 and 3 offer a low-emission approach with the integration of a carbon capture technology and an electrification alternative respectively. The evaluation carried out in this research indicates that Case 2 is the most environmentally favorable option, requiring the least energy input and producing the lowest CO_2 emissions per kilogram of hydrogen among the two low-carbon options. While Case 1 presents the highest environmental impact of the three cases, approximately 4.14 $kgCO_2/kgH_2$, its carbon footprint remains half of SMR with out carbon capture. Case 3, though requiring the highest energy input due to the electric arc furnace technology, achieves a carbon footprint comparable to that of Case 2.

A techno-economic assessment was conducted for the aforementioned proposals based on their levelized cost of hydrogen. The baseline alternative, Case 1, presented the lowest LCOH due to its simpler configuration, bringing a hydrogen cost of 2.54 USD/kgH_2. Case 2 with CCS resulted in the most affordable option considering a decarbonization measure with a levelized cost of 2.72 USD/kgH_2. These findings position scenario 2 as comparable to SMR with CCS and significantly more cost-effective than electrolysis. Moreover, Case 3 presents similar results to Case 2, with a slightly higher cost of 3.29 USD/kgH_2. Overall, all three proposed options offer economically viable pathways with added environmental benefits.

The techno-economic assessment for methane pyrolysis was evaluated considering regional characteristics of British Columbia. This province offers several favorable conditions for low-emission hydrogen

technologies such as low-carbon intensity electricity generation and natural gas availability. Regions with similar characteristics to BC should consider methane pyrolysis as a viable pathway to expand their hydrogen markets.

The potential of methane pyrolysis projects to provide a feasible solution for hydrogen economy has been analyzed in recent years. Although this technology is relatively noble and has some technical challenges, the presented techno-economic analysis supports the economic development of this new process by bringing a much lower carbon footprint compared to traditional methods at a competitive cost. The findings provided in this research support methane pyrolysis as an economically and environmentally favorable pathway, offering a promising bridge toward a sustainable, low-carbon hydrogen future.

REFERENCES

[1] M. Ball and M. Wietschel, "The future of hydrogen – opportunities and challenges," *Int. J. Hydrog. Energy*, vol. 34, no. 2, pp. 615–627, Jan. 2009, doi: 10.1016/j.ijhydene.2008.11.014.

[2] N. P. Brandon and Z. Kurban, "Clean energy and the hydrogen economy," *Philos. Trans. R. Soc. Math. Phys. Eng. Sci.*, vol. 375, no. 2098, p. 20160400, Jul. 2017, doi: 10.1098/rsta.2016.0400.

[3] D. J. Arent *et al.*, "Challenges and opportunities in decarbonizing the U.S. energy system," *Renew. Sustain. Energy Rev.*, vol. 169, p. 112939, Nov. 2022, doi: 10.1016/j.rser.2022.112939.

[4] R. Arjmand, J. Monroe, and M. McPherson, "The role of emerging technologies in Canada's electricity system transition," *Energy*, vol. 278, p. 127836, Sep. 2023, doi: 10.1016/j.energy.2023.127836.

[5] E. E. Michaelides, "Decarbonization of the electricity generation sector and its effects on sustainability goals," *Sustain. Energy Res.*, vol. 10, no. 1, p. 10, Aug. 2023, doi: 10.1186/s40807-023-00080-1.

[6] F. Alanazi, "Electric Vehicles: Benefits, Challenges, and Potential Solutions for Widespread Adaptation," *Appl. Sci.*, vol. 13, no. 10, p. 6016, May 2023, doi: 10.3390/app13106016.

[7] V. Balan, "Current Challenges in Commercially Producing Biofuels from Lignocellulosic Biomass," *ISRN Biotechnol.*, vol. 2014, pp. 1–31, May 2014, doi: 10.1155/2014/463074.

[8] J. F. Dallemand, G. De Santi, A. Leip, D. Baxter, N. Rettenmaier, and H. Ossenbrink, "Biomass for transport, heat and electricity: scientific challenges," *Manag. Environ. Qual. Int. J.*, vol. 21, no. 4, pp. 523–547, Jun. 2010, doi: 10.1108/14777831011049142.

[9] S. Griffiths, B. K. Sovacool, J. Kim, M. Bazilian, and J. M. Uratani, "Industrial decarbonization via hydrogen: A critical and systematic review of developments, socio-technical systems and policy options," *Energy Res. Soc. Sci.*, vol. 80, p. 102208, Oct. 2021, doi: 10.1016/j.erss.2021.102208.

[10] R. Borup, T. Krause, and J. Brouwer, "Hydrogen is Essential for Industry and Transportation Decarbonization," *Electrochem. Soc. Interface*, vol. 30, no. 4, pp. 79–84, Dec. 2021, doi: 10.1149/2.F18214IF.

[11] F. Chui, A. Elkamel, and M. Fowler, "An Integrated Decision Support Framework for the Assessment and Analysis of Hydrogen Production Pathways," *Energy Fuels*, vol. 20, no. 1, pp. 346–352, Jan. 2006, doi: 10.1021/ef050196u.

[12] M. Hermesmann and T. E. Müller, "Green, Turquoise, Blue, or Grey? Environmentally friendly Hydrogen Production in Transforming Energy Systems," *Prog. Energy Combust. Sci.*, vol. 90, p. 100996, May 2022, doi: 10.1016/j.pecs.2022.100996.

[13] M. P. Maniscalco, S. Longo, M. Cellura, G. Miccichè, and M. Ferraro, "Critical Review of Life Cycle Assessment of Hydrogen Production Pathways," *Environments*, vol. 11, no. 6, p. 108, May 2024, doi: 10.3390/environments11060108.

[14] J. D. Holladay, J. Hu, D. L. King, and Y. Wang, "An overview of hydrogen production technologies," *Catal. Today*, vol. 139, no. 4, pp. 244–260, Jan. 2009, doi: 10.1016/j.cattod.2008.08.039.

[15] S. Saeidi *et al.*, "Evolution paths from gray to turquoise hydrogen via catalytic steam methane reforming: Current challenges and future developments," *Renew. Sustain. Energy Rev.*, vol. 183, p. 113392, Sep. 2023, doi: 10.1016/j.rser.2023.113392.

[16] B. Amini Horri and H. Ozcan, "Green hydrogen production by water electrolysis: Current status and challenges," *Curr. Opin. Green Sustain. Chem.*, vol. 47, p. 100932, Jun. 2024, doi: 10.1016/j.cogsc.2024.100932.

[17] R. Yukesh Kannah *et al.*, "Techno-economic assessment of various hydrogen production methods – A review," *Bioresour. Technol.*, vol. 319, p. 124175, Jan. 2021, doi: 10.1016/j.biortech.2020.124175.

[18] S. R. Patlolla, K. Katsu, A. Sharafian, K. Wei, O. E. Herrera, and W. Mérida, “A review of methane pyrolysis technologies for hydrogen production,” *Renew. Sustain. Energy Rev.*, vol. 181, p. 113323, Jul. 2023, doi: 10.1016/j.rser.2023.113323.
[19] M. Shokrollahi, N. Teymouri, O. Ashrafi, P. Navarri, and Y. Khojasteh-Salkuyeh, “Methane pyrolysis as a potential game changer for hydrogen economy: Techno-economic assessment and GHG emissions,” *Int. J. Hydrog. Energy*, vol. 66, pp. 337–353, May 2024, doi: 10.1016/j.ijhydene.2024.04.056.
[20] Y. H. Chan *et al.*, “Thermal pyrolysis conversion of methane to hydrogen (H2): A review on process parameters, reaction kinetics and techno-economic analysis,” *Chin. Chem. Lett.*, vol. 35, no. 8, p. 109329, Aug. 2024, doi: 10.1016/j.cclet.2023.109329.
[21] A. Bhaskar, M. Assadi, and H. N. Somehsaraei, “Can methane pyrolysis based hydrogen production lead to the decarbonisation of iron and steel industry?,” *Energy Convers. Manag. X*, vol. 10, p. 100079, Jun. 2021, doi: 10.1016/j.ecmx.2021.100079.
[22] M. Dawkins, D. Saal, J. F. Marco, J. Reynolds, and S. Dann, “An iron ore-based catalyst for producing hydrogen and metallurgical carbon via catalytic methane pyrolysis for decarbonisation of the steel industry,” *Int. J. Hydrog. Energy*, vol. 48, no. 57, pp. 21765–21777, Jul. 2023, doi: 10.1016/j.ijhydene.2023.03.022.
[23] H. Alhamed *et al.*, “From methane to hydrogen: A comprehensive review to assess the efficiency and potential of turquoise hydrogen technologies,” *Int. J. Hydrog. Energy*, vol. 68, pp. 635–662, May 2024, doi: 10.1016/j.ijhydene.2024.04.231.
[24] J. Diab, L. Fulcheri, V. Hessel, V. Rohani, and M. Frenklach, “Why turquoise hydrogen will Be a game changer for the energy transition,” *Int. J. Hydrog. Energy*, vol. 47, no. 61, pp. 25831–25848, Jul. 2022, doi: 10.1016/j.ijhydene.2022.05.299.
[25] N. Sánchez-Bastardo, R. Schlögl, and H. Ruland, “Methane Pyrolysis for Zero-Emission Hydrogen Production: A Potential Bridge Technology from Fossil Fuels to a Renewable and Sustainable Hydrogen Economy,” *Ind. Eng. Chem. Res.*, vol. 60, no. 32, pp. 11855–11881, Aug. 2021, doi: 10.1021/acs.iecr.1c01679.
[26] Y. H. Chan *et al.*, “Thermal pyrolysis conversion of methane to hydrogen (H2): A review on process parameters, reaction kinetics and techno-economic analysis,” *Chin. Chem. Lett.*, vol. 35, no. 8, p. 109329, Aug. 2024, doi: 10.1016/j.cclet.2023.109329.
[27] Z. Fan, W. Weng, J. Zhou, D. Gu, and W. Xiao, “Catalytic decomposition of methane to produce hydrogen: A review,” *J. Energy Chem.*, vol. 58, pp. 415–430, Jul. 2021, doi: 10.1016/j.jechem.2020.10.049.
[28] M. McConnachie, M. Konarova, and S. Smart, “Literature review of the catalytic pyrolysis of methane for hydrogen and carbon production,” *Int. J. Hydrog. Energy*, vol. 48, no. 66, pp. 25660–25682, Aug. 2023, doi: 10.1016/j.ijhydene.2023.03.123.
[29] I. J. Okeke, B. A. Saville, and H. L. MacLean, “Low carbon hydrogen production in Canada via natural gas pyrolysis,” *Int. J. Hydrog. Energy*, vol. 48, no. 34, pp. 12581–12599, Apr. 2023, doi: 10.1016/j.ijhydene.2022.12.169.
[30] J. H. Gurney, “Building a case for the hydrogen economy,” *IEEE Power Energy Mag.*, vol. 2, no. 2, pp. 35–39, Mar. 2004, doi: 10.1109/MPAE.2004.1269615.
[31] S. Rodat, S. Abanades, J. Coulie, and G. Flamant, “Kinetic modelling of methane decomposition in a tubular solar reactor,” *Chem. Eng. J.*, vol. 146, no. 1, pp. 120–127, Jan. 2009, doi: 10.1016/j.cej.2008.09.008.
[32] N. Ozalp, K. Ibrik, and M. Al-Meer, “Kinetics and heat transfer analysis of carbon catalyzed solar cracking process,” *Energy*, vol. 55, pp. 74–81, Jun. 2013, doi: 10.1016/j.energy.2013.02.022.
[33] T. Keipi, T. Li, T. Løvås, H. Tolvanen, and J. Konttinen, “Methane thermal decomposition in regenerative heat exchanger reactor: Experimental and modeling study,” *Energy*, vol. 135, pp. 823–832, Sep. 2017, doi: 10.1016/j.energy.2017.06.176.

[34] D. Trommer, D. Hirsch, and A. Steinfeld, “Kinetic investigation of the thermal decomposition of CH4 by direct irradiation of a vortex-flow laden with carbon particles,” *Int. J. Hydrog. Energy*, vol. 29, no. 6, pp. 627–633, May 2004, doi: 10.1016/j.ijhydene.2003.07.001.
[35] L. J. J. Catalan and E. Rezaei, “Coupled hydrodynamic and kinetic model of liquid metal bubble reactor for hydrogen production by noncatalytic thermal decomposition of methane,” *Int. J. Hydrog. Energy*, vol. 45, no. 4, pp. 2486–2503, Jan. 2020, doi: 10.1016/j.ijhydene.2019.11.143.
[36] A. R. Razmi, A. R. Hanifi, and M. Shahbakhti, “Techno-economic analysis of a novel concept for the combination of methane pyrolysis in molten salt with heliostat solar field,” *Energy*, vol. 301, p. 131644, Aug. 2024, doi: 10.1016/j.energy.2024.131644.
[37] B. J. Leal Pérez, J. A. Medrano Jiménez, R. Bhardwaj, E. Goetheer, M. Van Sint Annaland, and F. Gallucci, “Methane pyrolysis in a molten gallium bubble column reactor for sustainable hydrogen production: Proof of concept & techno-economic assessment,” *Int. J. Hydrog. Energy*, vol. 46, no. 7, pp. 4917–4935, Jan. 2021, doi: 10.1016/j.ijhydene.2020.11.079.
[38] B. Parkinson, J. W. Matthews, T. B. McConnaughy, D. C. Upham, and E. W. McFarland, “Techno-Economic Analysis of Methane Pyrolysis in Molten Metals: Decarbonizing Natural Gas,” *Chem. Eng. Technol.*, vol. 40, no. 6, pp. 1022–1030, Jun. 2017, doi: 10.1002/ceat.201600414.
[39] M. E. Tabat *et al.*, “Process design, exergy, and economic assessment of a conceptual mobile autothermal methane pyrolysis unit for onsite hydrogen production,” *Energy Convers. Manag.*, vol. 278, p. 116707, Feb. 2023, doi: 10.1016/j.enconman.2023.116707.
[40] A. Al-Qahtani, B. Parkinson, K. Hellgardt, N. Shah, and G. Guillen-Gosalbez, “Uncovering the true cost of hydrogen production routes using life cycle monetisation,” *Appl. Energy*, vol. 281, p. 115958, Jan. 2021, doi: 10.1016/j.apenergy.2020.115958.
[41] D. Milani, A. Kiani, and R. McNaughton, “Renewable-powered hydrogen economy from Australia’s perspective,” *Int. J. Hydrog. Energy*, vol. 45, no. 46, pp. 24125–24145, Sep. 2020, doi: 10.1016/j.ijhydene.2020.06.041.
[42] Enbridge Gas, “Learn About Natural Gas | Enbridge Gas.” Accessed: Oct. 18, 2024. [Online]. Available: https://www.enbridgegas.com/about-enbridge-gas/learn-about-natural-gas
[43] G. Towler, *Chemical engineering design*, 6th edition. Waltham, MA: Elsevier, 2019.
[44] K. M. Guthrie, “Chemical Engineering: Capital Cost Estimating,” in *Chemical Engineering*, 6th ed., vol. 76, 1969, p. 114.
[45] J. M. Douglas, *Conceptual design of chemical processes*. in McGraw-Hill chemical engineering series. New York: McGraw-Hill, 1988.
[46] L. Chan, “Industry Reports | The Potential for Methane Pyrolysis in BC | CICE,” B.C. Centre for Innovation and Clean Energy. Accessed: Oct. 23, 2024. [Online]. Available: https://cice.ca/knowledge-hub/the-potential-for-methane-pyrolysis-in-b-c-report/
[47] Canada Environment and Climate Change, “Pre-publication: Updated carbon intensity of natural gas and propane.” Accessed: Oct. 23, 2024. [Online]. Available: https://www.canada.ca/en/environment-climate-change/services/managing-pollution/fuel-life-cycle-assessment-model/updated-carbon-intensity-natural-gas-propane.html
[48] Ministry of Environment and Climate Change, “Electricity emission intensity factors for grid-connected entities - Province of British Columbia.” Accessed: Oct. 23, 2024. [Online]. Available: https://www2.gov.bc.ca/gov/content/environment/climate-change/industry/reporting/quantify/electricity
[49] B.C. Centre for Innovation and Clean Energy, “The Potential for Methane Pyrolysis in B.C. Report,” 2024.
[50] Canada Environment and Climate Change, “The federal carbon pollution pricing benchmark.” Accessed: Oct. 23, 2024. [Online]. Available: https://www.canada.ca/en/environment-climate-change/services/climate-change/pricing-pollution-how-it-will-work/carbon-pollution-pricing-federal-benchmark-information.html

[51] M. Katebah, M. Al-Rawashdeh, and P. Linke, “Analysis of hydrogen production costs in Steam-Methane Reforming considering integration with electrolysis and CO2 capture,” *Clean. Eng. Technol.*, vol. 10, p. 100552, Oct. 2022, doi: 10.1016/j.clet.2022.100552.
[52] A. A. Abd, M. R. Othman, H. S. Majdi, and Z. Helwani, “Green route for biomethane and hydrogen production via integration of biogas upgrading using pressure swing adsorption and steam-methane reforming process,” *Renew. Energy*, vol. 210, pp. 64–78, Jul. 2023, doi: 10.1016/j.renene.2023.04.041.
[53] M. F. U. Hasnain *et al.*, “Optimization and Techno-Economic analysis of catalytic gasification of wheat straw biomass using ASPEN PLUS model,” *Arab. J. Chem.*, vol. 17, no. 7, p. 105821, Jul. 2024, doi: 10.1016/j.arabjc.2024.105821.
[54] M. Singh, S. A. Salaudeen, B. H. Gilroyed, and A. Dutta, “Simulation of biomass-plastic co-gasification in a fluidized bed reactor using Aspen plus,” *Fuel*, vol. 319, p. 123708, Jul. 2022, doi: 10.1016/j.fuel.2022.123708.
[55] M. Shokrollahi, N. Teymouri, O. Ashrafi, P. Navarri, and Y. Khojasteh-Salkuyeh, “Methane pyrolysis as a potential game changer for hydrogen economy: Techno-economic assessment and GHG emissions,” *Int. J. Hydrog. Energy*, vol. 66, pp. 337–353, May 2024, doi: 10.1016/j.ijhydene.2024.04.056.

APPENDIX A

Table 11. Methane pyrolysis equipment sizing evaluation

Tag	Parameter Definition	Sizing Value			Unit	Reference
		A	B	C		
EA-101	Effective Surface Area	117.2			m^2	[43]
EA-103	Effective Surface Area	32.0			m^2	[43]
EA-104	Effective Surface Area	11.2	16.6	11.3	m^2	[43]
EA-106	Effective Surface Area	520.7			m^2	[43]
EA-107	Effective Surface Area	26.5			m^2	[43]
EA-108	Effective Surface Area	27.9	11.6	37.4	m^2	[43]
EA-105	Solids capacity	6.205			ton/h	[37]
EA-102	Heat Flow	4.66			MW	[43]
PR-101	Heat Flow	13.1			MW	[43]
CYC-101	Volumetric Flow, V	8072			ft^3/min	[44]
K-101	Compressor power	1099	1064	1086	kWe	[43]
B-101	Actual Volume Flow	10228			m3/h	[43]
B-102	Actual Volume Flow	30683			m3/h	[43]
K-102	Compressor power	283.1	261.6	238.9	kWe	[43]
K-103	Compressor power	295.1			kWe	[43]
PSA-101	Purge gas flow	166.0			kmol/h	[37]
P-101	Actual Volume Flow	98.5			m^3/h	[43]
P-102	Actual Volume Flow	147.8			m^3/h	[43]
P-103	Actual Volume Flow	27.7			m^3/h	[43]
P-104	Actual Volume Flow	64.1			m^3/h	[43]
SILO-101	Volumetric Storage, V	22421			ft^3	[44]
MEA-101	CO2 captured flow	2.236			kg/s	[37]
EAF-101	Net electric power	63894447			kJ/h	[37]

APPENDIX B

Table 12. Methane pyrolysis total equipment cost

Tag	Equipment Type	Units	Total Equipment Cost (Purchased + Installation)		
			Case 1	Case 2	Case 3
EA-101	Heat Exchanger (U-tube S&T)	USD	285,328	285,328	271,940
EA-103	Heat Exchanger (U-tube S&T)	USD	202,458	202,458	203,122
EA-104	Heat Exchanger (U-tube S&T)	USD	563,697	563,697	563,697
EA-106	Heat Exchanger (U-tube S&T)	USD	-	809,112	-
EA-107	Heat Exchanger (U-tube S&T)	USD	-	198,002	-
EA-108	Heat Exchanger (U-tube S&T)	USD	-	593,025	-
EA-105	Solex Heat Exchanger	USD	2,066,484	2,066,484	2,066,484
EA-102	Direct-fired Heater Furnace	USD	1,815,556	1,815,556	-
PR-101	Pyrolysis Process Furnace	USD	3,909,337	3,909,337	-
CYC-101	Solid-gas Cyclone	USD	542,676	542,676	542,676
K-101	Reciprocating Compressor	USD	9,830,703	9,830,703	9,830,703
B-101	Air Blower	USD	415,130	415,130	-
B-102	Air Blower	USD	972,920	972,920	-
K-102	Reciprocating Compressor	USD	-	14,478,216	-
K-103	Reciprocating Compressor	USD	-	-	1,922,488
PSA-101	Pressure Swing Adsorption	USD	10,036,908	10,036,908	8,657,930
P-101	Water pump	USD	54,852	54,852	54,852
P-102	Water pump	USD	63,787	63,787	63,787
P-103	Water pump	USD	41,043	41,043	41,043
P-104	Water pump	USD	-	48,332	-
SILO-101	Hopper Carbon Storage	USD	4,007,455	4,007,455	4,007,455
MEA-101	MEA CCS Technology	USD	-	14,744,443	-
EAF-101	Electric Arc Furnace	USD	-	-	58,907,272